

4-2015

# Robust Recognition using L1-Principal Component Analysis

Matthew Johnson

Follow this and additional works at: <http://scholarworks.rit.edu/theses>

---

## Recommended Citation

Johnson, Matthew, "Robust Recognition using L1-Principal Component Analysis" (2015). Thesis. Rochester Institute of Technology. Accessed from

This Thesis is brought to you for free and open access by the Thesis/Dissertation Collections at RIT Scholar Works. It has been accepted for inclusion in Theses by an authorized administrator of RIT Scholar Works. For more information, please contact [ritscholarworks@rit.edu](mailto:ritscholarworks@rit.edu).

# **Robust Recognition using L1-Principal Component Analysis**

by

**Matthew Johnson**

A Thesis Submitted in Partial Fulfillment of the Requirements for the Degree of  
Master of Science in Computer Engineering

Supervised by

Dr. Andreas Savakis  
Department of Computer Engineering  
Kate Gleason College of Engineering  
Rochester Institute of Technology  
Rochester, NY  
April 2015

**Approved By:**

---

Dr. Andreas Savakis  
*Primary Advisor – R.I.T. Department of Computer Engineering*

---

Dr. Sonia Lopez Alarcon  
*Committee Member – R.I.T. Department of Computer Engineering*

---

Dr. Raymond Ptucha  
*Committee Member – R.I.T. Department of Computer Engineering*

# **Dedication**

I would like to thank my family, I am forever grateful for your words of encouragement and unwavering support.

# Acknowledgements

I would like to thank my advisor Dr. Andreas Savakis for his assistance and mentorship in the process of developing this thesis. I would also like to thank my committee members Dr. Sonia Lopez Alarcon and Dr. Raymond Ptucha. Additionally I want to thank my colleagues in the Computer Vision Lab Breton Minnehan and Sriram Kumar, who were invaluable resources throughout this process.

## Abstract

The wide availability of visual data via social media and the internet, coupled with the demands of the security community have led to an increased interest in visual recognition. Recent research has focused on improving the accuracy of recognition techniques in environments where variability is well controlled. However, applications such as identity verification often operate in unconstrained environments. Therefore there is a need for more robust recognition techniques that can operate on data with considerable noise.

Many statistical recognition techniques rely on principal component analysis (PCA). However, PCA suffers from the presence of outliers due to occlusions and noise often encountered in unconstrained settings. In this thesis we address this problem by using  $L_1$ -PCA to minimize the effect of outliers in data.  $L_1$ -PCA is applied to several statistical recognition techniques including eigenfaces and Grassmannian learning. Several popular face databases are used to show that  $L_1$ -Grassmann manifolds not only outperform, but are also more robust to noise and occlusions than traditional  $L_2$ -Grassmann manifolds for face and facial expression recognition. Additionally a high performance GPU implementation of  $L_1$ -PCA is developed using CUDA that is several times faster than CPU implementations.

## Table of Contents

Chapter 1	Introduction .....	1
Chapter 2	Background.....	4
2.1.	Principal Component Analysis .....	4
2.1.1	L2-PCA .....	4
2.1.2	L1-PCA .....	7
2.2.	PCA Recognition.....	10
2.3.	Grassmannian Recognition.....	13
2.4.	LBP/LTP Features .....	16
2.5.	GPU Acceleration.....	18
2.5.1	General Purpose GPU Computing .....	18
2.5.2	GPU accelerated L1-PCA .....	21
Chapter 3	L1-PCA Recognition .....	22
3.1.	L1-PCA Algorithm Design.....	22
3.2.	Recognition Techniques .....	24
3.2.1	L1-Eigenfaces.....	24
3.2.2	L1-Grassmann .....	26
3.2.3	LTP Features .....	27
3.3.	CPU Implementation .....	28
3.4.	GPU Implementation.....	31

Chapter 4	Experimental Results .....	36
4.1.	Experimental Setup.....	36
4.2.	Datasets.....	36
4.2.1	Yale Face Database .....	36
4.2.2	AT&T Database of Faces.....	38
4.2.3	Extended Yale Face Database B .....	39
4.2.4	AR Face Database .....	40
4.2.5	Labeled Faces in the Wild Database .....	41
4.2.6	Cohn-Kanade Databases .....	42
4.3.	Parameter Selection .....	43
4.4.	Accuracy Tests .....	44
4.5.	Accuracy State of the Art .....	61
4.5.1	Yale Face Database .....	62
4.5.2	AT&T Database of Faces.....	63
4.5.3	Extended Yale Face Database B .....	63
4.5.4	AR Face Database .....	64
4.6.	Speed tests .....	65
Chapter 5	Conclusion and Future Work.....	69
Bibliography	.....	72

## List of Figures

Figure 1: Multivariate Gaussian with Two Principal Components .....	4
Figure 2: L1-PCA Toy Example.....	7
Figure 3: First Ten Eigenpictures .....	11
Figure 4: Grassmann Manifold Mapping.....	13
Figure 5: LBP Operator .....	16
Figure 6: LTP Operator.....	17
Figure 7: CPU Architecture (left) vs GPU Architecture (right) .....	18
Figure 8: L1-PCA Algorithm Flow.....	23
Figure 9: Eigenfaces from Occluded Dataset .....	24
Figure 10: Rectangular Noise on Yale Dataset.....	25
Figure 11: Recognition using Grassmann Manifolds .....	27
Figure 12: LTP Preprocessing .....	28
Figure 13: CPU Tree Reduction .....	30
Figure 14: GPU Kernel Flow .....	33
Figure 15: GPU Reduction.....	34
Figure 16: Min Reduction Kernel .....	35
Figure 17: Yale Face Database Images Across Two Subjects.....	37
Figure 18: Yale Face Database Sample Image from each Subject .....	37
Figure 19: AT&T Database Images Across Two Subjects.....	38
Figure 20: AT&T Database Sample Image from each Subject .....	38
Figure 21: Extended Yale Face Database B Images Across Two Subjects .....	39



Figure 22: Extended Yale Face Database B Sample Image from each Subject ...	39
Figure 23: AR Face Database Sample Image from each Subject .....	40
Figure 24: AR Face Database Images Across a Subject.....	41
Figure 25: LFW Face Database Images Across Two Subjects.....	41
Figure 26: : LFW Face Database Subjects with at Least 20 Images .....	42
Figure 27: Emotions from the Extended Cohn-Kanade Database .....	42
Figure 28: Eigenface Comparison Test Yale Database .....	45
Figure 29: Eigenface Comparison Test AT&T Database .....	45
Figure 30: Grassmann Comparison Test Yale Database .....	46
Figure 31: Grassmann Comparison Test AT&T Database .....	46
Figure 32: Grassmann Comparison Test Extended Yale B Database.....	47
Figure 33: Eigenfaces Comparison Test Occluded Yale Database .....	48
Figure 34: Eigenfaces Comparison Test Occluded AT&T Database .....	48
Figure 35: Grassmann Comparison Test Occluded Yale Database .....	49
Figure 36: Grassmann Comparison Test Occluded AT&T Database.....	49
Figure 37: Grassmann Comparison Test Occluded Extended Yale.....	50
Figure 38: LTP L2-Eigenface $t$ Test for Yale Database .....	51
Figure 39: LTP L1-Eigenface $t$ Test for Yale Database .....	51
Figure 40: LTP Eigenfaces Test Yale Database ( $t = 2$ ) .....	52
Figure 41: LTP Eigenfaces Test AT&T Database ( $t = 6$ ).....	53
Figure 42: LTP Eigenfaces Test Extended Yale B Database ( $t = 1$ ) .....	53
Figure 43: LTP Grassmann Test Yale Database ( $t = 5$ ).....	54
Figure 44: LTP Grassmann Test AT&T Database ( $t = 6$ ) .....	54

Figure 45: LTP Grassmann Test Extended Yale B Database ( $t = 5$ ) .....	55
Figure 46: LTP Grassmann Yale Database ( $t = 5$ ).....	57
Figure 47: LTP Grassmann AT&T Database ( $t = 6$ ) .....	57
Figure 48: LTP Grassmann Extended Yale B Database ( $t = 5$ ).....	58
Figure 49: LTP Grassmann AR Database ( $t = 5$ ).....	58
Figure 50: LTP Grassmann LFW Database ( $t = 5$ ).....	59
Figure 51: LTP Grassmann Cohn-Kanade Database ( $t = 14$ ).....	59
Figure 52: LTP Grassmann Extended Cohn-Kanade Database ( $t = 16$ ).....	60
Figure 53: LTP Grassmann Comparison on Varying number of Subject Images	61
Figure 54: CPU Timing .....	66
Figure 55: GTX Timing.....	66
Figure 56: Tesla Timing.....	67
Figure 57: GTX Speedup .....	67
Figure 58: Tesla Speedup.....	68

## List of Tables

Table 1: Grassmann Distance Metrics .....	15
Table 2: State of the Art Comparison for Yale Face Database .....	62
Table 3: State of the Art Comparison for AT&T Database of Faces.....	63
Table 4: State of the Art Comparison for Extended Yale B Face Database .....	64
Table 5: State of the Art Comparison for AR Face Database .....	64

## Glossary

<b>CPU</b>	Central Processing Unit
<b>GPU</b>	Graphics Processing Unit
<b>ALU</b>	Arithmetic Logic Unit
<b>DRAM</b>	Dynamic Random-Access Memory
<b>GPGPU</b>	General-purpose Computing on Graphics Processing Units
<b>SIMD</b>	Single Instruction Multiple Data
<b>SM</b>	Streaming Multiprocessors
<b>SP</b>	Streaming Processors
<b>CUDA</b>	Compute Unified Device Architecture
<b>BLAS</b>	Basic Linear Algebra Subprograms
<b>LBP</b>	Local Binary Patterns
<b>LTP</b>	Local Ternary Patterns

## Chapter 1 Introduction

Recent research has focused on increasing the accuracy of recognition techniques, however little effort has been devoted to increasing robustness. Applications such as surveillance often operate in unconstrained environments where subjects may be partially occluded by objects such as glasses and scarfs. Thus, there is a significant need for face recognition techniques that are not only accurate, but also robust to noise.

Many recognition techniques today rely on statistical techniques that perform direct correlation comparisons between the test face and training databases [1]. To improve performance many techniques relay on PCA to both reduce dimensionality and determine better feature subspaces. One of the limitations of PCA is its sensitivity to outliers, as the  $L_2$ -norm has the tendency to exaggerate the influence of noise over valid data.  $L_1$ -PCA utilizes the  $L_1$ -norm and as a result is more robust to noise. However, there is no direct solution for  $L_1$ -PCA and iterative solutions must contend with the non-linear search space. As a result of these limitations, researchers have focused on using suboptimal solutions to speedup  $L_1$ -PCA.

Although suboptimal solutions have improved the speed of  $L_1$ -PCA, CPU implementations still struggle with large datasets. Recently researchers have begun to utilize general purpose graphics processing units (GPGPU) to speedup algorithms that are too computationally intensive for CPU processing alone. The GPU's single instruction multiple data architecture achieves large speedups when an algorithm has a high degree of data level parallelism. Some early work has shown that the CUDA architecture shows potential for  $L_1$ -PCA [2].

Grassmannian learning is an example of a recognition technique that would benefit from  $L_1$ -PCA. The Grassmann manifold has been investigated for variety of recognition applications, including object, action and face recognition [3], [4]. This technique maps data subspaces to points on the manifold using PCA. The Grassmann manifold's unique geometric structure promotes high class discrimination and compensates for missing data allowing for great recognition accuracy. However, the PCA mapping used for Grassmann manifolds is sensitive to outliers and could be improved with  $L_1$ -PCA.

The contributions of this thesis are the following. The first contribution is an extension of an efficient  $L_1$  principal component algorithm to multiple components that demonstrates a high degree of robustness to noise. The second contribution is a  $L_1$ -PCA mapping for Grassmann manifolds that can improve accuracy and reduce the effects of noise in both face and facial expression recognition. The third contribution is an extension of  $L_1$ -Grassmann using local ternary patterns which improves robustness to variations of illuminations. The final contribution is a high performance implementation of the  $L_1$ -PCA on a GPU using CUDA. This GPU implementation is suitable for recognition on databases that CPU implementations would not be able to run in a reasonable amount of time.

This document is organized as follows: Chapter 2 discusses the prior work done in  $L_1$ -PCA and the recognition algorithms used throughout the thesis. Chapter 3 discusses the how to accelerate proposed  $L_1$ -PCA algorithm and details the  $L_1$  versions of the face and facial expression recognition algorithms. Chapter 4 details the experiments performed to benchmark the proposed  $L_1$ -PCA algorithm as well as the results of the face

and facial expression recognition algorithms. Chapter 5 provides a conclusion as well as potential areas for future work.

## Chapter 2 Background

This chapter outlines related work in recognition,  $L_1$ -PCA and high performance implementations of  $L_1$ -PCA. In Section 2.1 the formulation for  $L_2$ -PCA is presented and the previous work on  $L_1$ -PCA is discussed. Previous work in recognition is discussed in Sections 2.2, 2.3 and 2.4. In section 2.5 GPGPU and how others have leveraged the GPU for accelerating  $L_1$ -PCA algorithms is discussed.

### 2.1. Principal Component Analysis

#### 2.1.1 L2-PCA

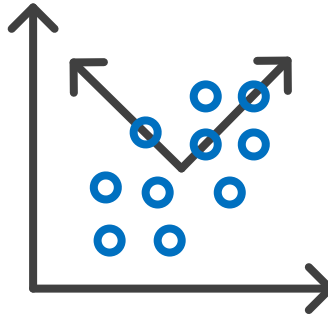


Figure 1: Multivariate Gaussian with Two Principal Components

Principal component analysis was first introduced by Karl Pearson in 1901 and has been used in a variety of fields including signal processing, pattern recognition and computer vision [5]. The goal of principal component analysis is to find a set of  $M$  orthogonal vectors aligned in the directions of maximum variance of the data such that  $M \leq D$ , where  $D$  is the dimensionality of the data. Figure 1 shows the first two principal components from a multivariate normal distribution. This process often reveals the



underlying structure of data and allows complex datasets to be represented in a lower dimensionality.

This set of orthogonal vectors are known as eigenvectors or principal components and can be represented as the matrix  $R \in \Re^{D \times M}$  where each column is a principal component aligned with the direction of maximum variance.

Traditional PCA utilizes the  $L_2$ -norm which is defined as

$$d_{L_2} = \|\mathbf{v}\|_2 = \sqrt{\sum_{i=0}^{n-1} \mathbf{v}_i^2} \quad (2.1)$$

where  $\mathbf{v} \in \Re^{n \times 1}$ . One way to solve for  $L_2$  principal components is by finding the set of vectors  $R \in \Re^{D \times M}$  that minimize the  $L_2$ -distance between the original signal and its reconstruction

$$E_2(R, V) = \arg \min \|X - RV\|_2 \quad (2.2)$$

where data matrix  $X \in \Re^{D \times N}$ , whose columns are data samples such that there are  $N$  data samples and  $V \in \Re^{M \times N}$  is the coefficient matrix given by

$$V = R^T X \quad (2.3)$$

without loss of generality, we can assume  $X$  is centered such that the set of samples  $\{x_i\}_{i=1}^N$  has zero mean. Using the projection theorem (2.2) can be rewritten as the following optimization problem

$$R_{L_2} = \arg \min \|X - RR^T X\|_2 \quad (2.4)$$

Traditionally (2.2) is solved by performing eigen-decomposition on the covariance matrix of  $X$ . The covariance matrix describes the relationships between pairs of measurements in a dataset [6]. The diagonal elements are the variances across features

and the off diagonal elements are the covariance between features. The covariance matrix is given by

$$S_X = \frac{1}{n-1} XX^T \quad (2.5)$$

The PCA process minimizes the square error of the reconstruction, and this is equivalent to maximizing the captured variance [6]. Eigendecomposition finds a set of orthonormal vectors that diagonalize the covariance matrix. A single principal component can be solved using the characteristic equation

$$S_X r_{L_2} = \lambda r_{L_2} \quad (2.6)$$

where  $\lambda$  is the eigenvalue corresponding to eigenvector  $r_{L_2}$ . Since the covariance matrix is symmetric it can be decomposed to

$$S_X = R_{L_2} \Sigma^2 R_{L_2}^T \quad (2.7)$$

where  $\Sigma^2$  is a diagonal matrix containing the variance of each eigenvector in  $R_{L_2}$ . Another way to solve for the principal components is to maximize the trace of  $\Sigma^2$  from (2.7). This in turn maximizes the variance along the diagonal and solves for the eigenvectors thus it can be rewritten as

$$R_{L_2} = \operatorname{argmax} \operatorname{Trace}(R^T S_X R) \quad (2.8)$$

since  $\|A\|_2^2 = \operatorname{Trace}(A^T A)$  [7], (2.8) can be rewritten into its final form

$$R_{L_2} = \operatorname{arg max} \|X^T R\|_2 \quad (2.9)$$

This reformulation is known as the projection energy maximization. Equations (2.2), (2.4) and (2.9) are  $L_2$  equivalent optimization problems [7].

### 2.1.2 L1-PCA

In  $L_1$ -PCA we find a set of orthogonal vectors that are aligned in the direction of maximum variance with respect to the  $L_1$ -norm. The  $L_1$ -norm of vector  $\mathbf{v}$  is given by

$$d_{L1} = \|\mathbf{v}\|_1 = \sum_{i=0}^{n-1} |v_i| \quad (2.10)$$

The main advantage of the  $L_1$ -norm is its robustness to outliers. In  $L_2$ -PCA outliers with a large norm are exaggerated by the use of the  $L_2$ -norm [8]. Figure 2 highlights the effect of outliers on  $L_2$ -PCA in a toy scenario.

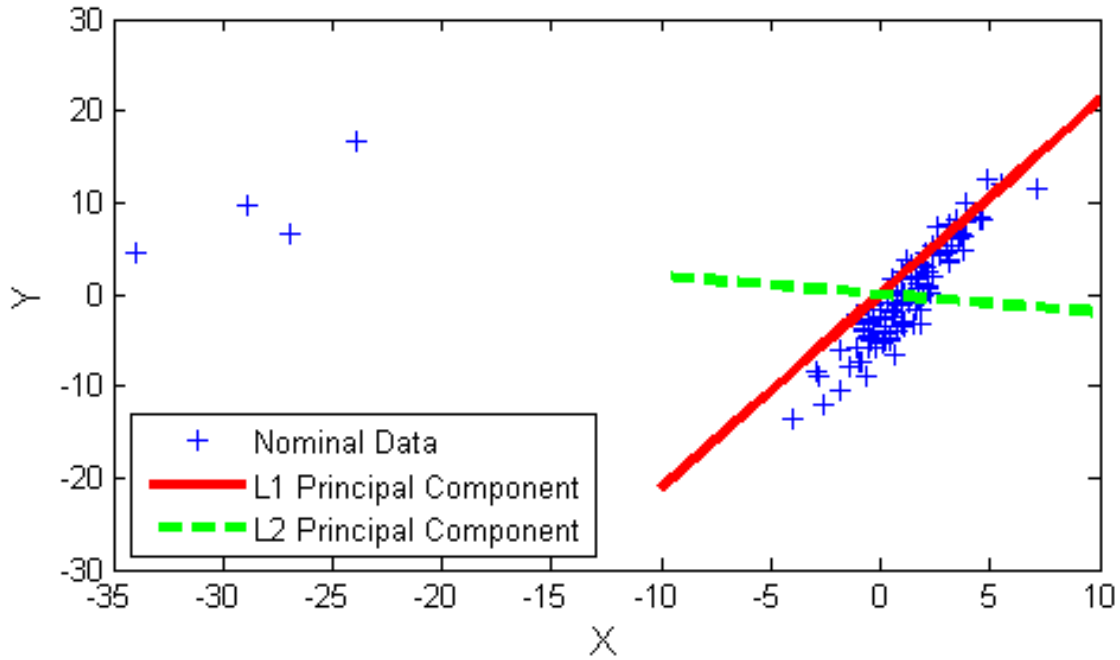


**Figure 2: L1-PCA Toy Example**

Outliers (left side), L2-PCA (dotted line) and L1-PCA (solid line)

A multivariate Gaussian was used to generate test points and then four of those points had noise added to them. Both  $L_2$ -PCA and  $L_1$ -PCA were used to find the first principal

component of the data. As shown in Figure 2,  $L_2$ -PCA was heavily influenced by the outliers, while  $L_1$ -PCA offered a more accurate representation of the data. The three equivalent  $L_2$  optimization problems (2.2), (2.4) and (2.9) can be translated to the  $L_1$ -norm and used to solve for the  $L_1$ -principal components [7].

$$E_1(R, V) = \arg \min |X - RV|_1 \quad (2.11)$$

$$R_{L_1} = \arg \min |X - RR^T X|_1 \quad (2.12)$$

$$R_{L_1} = \arg \max |X^T R|_1 \quad (2.13)$$

Under the  $L_1$ -norm the above optimization problems are no longer equivalent because the PCA scalability property does not hold due to the loss of the projection theorem [9].

In [10], Ke et al. use the error minimization in (2.11) to solve for the  $L_1$  principal components. Ke et al. solves this problem by utilizing alternating convex minimization. The  $L_1$ -norm cost function in (2. 11) is not generally convex, however if  $R$  or  $V$  is known then the problem becomes convex [10]. Utilizing this scheme Ke et al. optimizes (2. 11) by alternating between optimizing  $R$  and  $V$  using convex minimization.

Several researchers have explored using the  $L_1$  projection energy optimization in (2.13) for  $L_1$ -PCA. In [8], Kwak introduced a suboptimal approach called PCA- $L_1$  that iteratively solves the energy maximization problem. Kwak's algorithm solves for a single eigenvector by using the optimal polarity to iteratively converge to a vector that maximizes the  $L_1$  projection energy. The remaining eigenvectors are solved for in a greedy manner by removing the previous eigenvectors contribution from each data sample as follows

$$x_i^{(update)} = x_i - r_{L_1}(r_{L_1}^T x_i) \quad \forall i \in \{1, \dots, N\} \quad (2.14)$$

Kwak's greedy search algorithm does not guarantee an optimal solution, however it does guarantee the orthonormality of all principal components and that the set of principal components will maximize  $L_1$  dispersion [8]. The computational complexity of  $L_1$ -PCA with greedy search is  $O(MNDT)$  where  $T$  is the number of iterations to converge. The main issue with Kwak's solution is that the computational complexity is dependent on the dimensionality of the data which is equivalent to the number of pixels in an image for face recognition. In [11], Nie et al. replaced the greedy search method introduced by Kwak with a non-greedy method. Kwak's PCA- $L_1$  algorithm is extended to solve for a set of  $L_1$  eigenvectors simultaneously. The Nie et al. solution does not guarantee convergence to an optimal  $L_1$ -subspace and has the same time complexity as PCA- $L_1$  with greedy search. However Nie et al. has experimentally shown that this non-greedy approach outperforms the greedy approach on several datasets [11]. In [9], Markopoulos et al. proves that a single  $L_1$  principal component can be solved for using

$$r_{L_1} = \frac{Xb_{opt}}{\|Xb_{opt}\|_2} \quad (2.15)$$

where

$$b_{opt} = \arg \max_{b \in \{\pm 1\}^N} \|Xb\|_2 = \arg \max_{b \in \{\pm 1\}^N} b^T X^T X b \quad (2.16)$$

This proof reformulates the  $L_1$  projection energy optimization as a search over a binary vector. Markopoulos et al. show that the optimal set of  $L_1$  principal components can be solved by exhaustive searching  $2^{MN}$  binary matrices of size  $N \times M$ . Additionally in [9] Markopoulos et al. show that in the special case  $N \geq D$  an orthonormal scanning matrix can be used to solve for an optimal set of  $L_1$  principal components in polynomial time. In

subsequent work, Kundu et al. introduced a fast suboptimal method for the computation of a single  $L_1$ -principal component for real-valued data [12]. This algorithm optimizes (2.16) using greedy bit flipping. The binary vector is optimized by identifying bits that negatively contribute to the  $L_1$  projection energy and flipping them. The  $L_1$  projection energy associated with (2.16) can be written as

$$b^T X^T X b = \text{Trace}(X^T X) + \sum_i 2b_i \left\{ \sum_{j>i} b_j (X^T X)_{i,j} \right\} \quad (2.17)$$

where  $i$  and  $j$  vary from 1 to  $N$ . From (2.17) Kundu et al. [12] show that the contribution of the  $i^{\text{th}}$  bit to the aggregative maximum is given by

$$\alpha_i = \pm 4b_i \sum_{j \neq i} b_j (X^T X)_{i,j} \quad (2.18)$$

This bit flipping is repeated until all bits positively contribute towards the aggregative maximum or until the maximum number of iterations are reached. This process can be repeated up to  $N$  times using the sign of the columns of the covariance matrix as the initial values for the binary vectors. The binary vector candidate with the largest projection energy is determined using (2.16) and the corresponding eigenvector is obtained from (2.15).

## 2.2. PCA Recognition

In [13] Kirby et al. showed that principal component analysis could be used to generate a set of basis features called eigenpictures. In their algorithm they used a set of face images that was centered such that the eyes of each person were aligned. Next the images are vectorized to form a column vector with a size equal to the number of pixels

in the image. A set of eigenpictures is generated by running principal component analysis (PCA) on the column vectors as shown in Figure 3. PCA discovers the underlying Euclidian structure in the data and utilizes that to reduce the dimensionality and hopefully increase class discrimination. These eigenpictures form a basis and are used to transfer images to a smaller dimensional feature space. Once in feature space direct correlation comparisons between the test and training images is used to perform recognition.



**Figure 3: First Ten Eigenpictures**

In [14] Turk et al. coined the term eigenfaces when they applied Kirby's et al. eigenpictures to face recognition. Turk et al. starts of by calculating the eigenfaces using the same procedure as Kirby et al. The eigenfaces are then sorted using their corresponding eigenvalues from largest to smallest and a subset is formed using the eigenvectors with the largest eigenvalues. The larger eigenvalues correspond to eigenfaces that capture more variance and as a result are better basis vectors. This subset of eigenvectors is used to transform training and test images into face space using the

projection theorem. Once in face space the Euclidean distance between a test image and a face class is used for recognition. Unfortunately, traditional eigenfaces are not robust to large variations in illumination, pose, facial expression and the presence of occlusions.

Numerous extensions to eigenfaces have been proposed to overcome its limitations. Modular eigenfaces is one such extension that is more robust to occlusions, variations in illumination and facial expression. Modular eigenfaces was first introduced by Pentland et al in [15]. Pentland et al in divided both eyes, the nose and the mouth into sub-images and then ran principal component analysis on each sub-image across the training set [15]. This results in a set of eigenvectors for each sub-image. Similar to traditional eigenfaces a subset is formed using the eigenvectors with the largest eigenvalues for each sub-image. The subsets of eigenvectors is used to transform each sub-image in the training and test images into an alternate space using the projection theorem. After that the alternate space weights for each sub-image are concatenated into a single descriptor. Pattern recognition techniques are then applied to these descriptors to perform face recognition.

The advantage of modular eigenfaces is that by dividing the image areas with very different illumination or areas with noise wont effect the other sub-images projection. In [16] Gottumukkal et al. extended Pentland et al. work by dividing the entire image into sub-images, instead of only using the eyes and mouth images. By dividing the entire image only a subset of the sub-images would be affected by the variations in illumination and as a result would be more robust.

In [17], Yang et al. introduced 2D-eigenfaces, another extension to the traditional eigenfaces technique that improves recognition accuracy and reduces computation time.



This technique utilizes 2D-PCA to calculate eigenfaces using the image covariance matrix. This matrix can more efficiently capture the relationships between images, as opposed to traditional PCA which needs to vectorize the image before computing the covariance matrix. Yang et al. demonstrates that 2D-PCA outperforms traditional PCA, but requires more eigenvectors [17].

### 2.3. Grassmannian Recognition

The Grassmann manifold  $G(m, D)$  strives to reduce the dimensionality of data by finding a lower dimensional space to represent the data. This is achieved by representing  $m$  linear subspaces of  $\mathbb{R}^D$  as  $m$  points on the manifold. Points on the Grassmann manifold can be formed from entire datasets, class examples, or a single data point. Data is mapped onto the Grassmann manifold by forming a dictionary  $X = [x_1, \dots, x_N] \in \mathbb{R}^{D \times N}$  whose columns are data samples, where  $D$  is the dimensionality of the data and  $N$  is the number of data samples. From the dictionary  $X$  a unit vector representation needs to be generated. Traditionally this is done using  $L_2$  principal component analysis as shown in Figure 4.

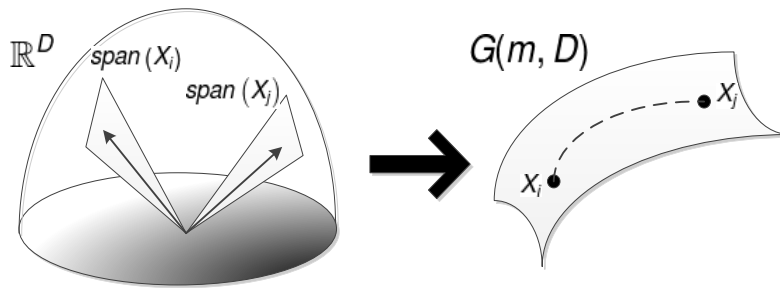


Figure 4: Grassmann Manifold Mapping

A subspace mapping from a Euclidian space (left) to a Grassmann manifold (right).

The Grassmann manifold is naturally a smooth curved surface and as a result Euclidian distance metrics cannot be directly applied. Several different distance metrics have been explored for Grassmann manifolds based on principal angles between subspaces  $\theta = [\theta_1, \theta_2, \dots, \theta_m]$ , where the principal angle between two subspaces is given using SVD such that

$$x_1'x_2 = USV' \quad (2.19)$$

$$diag(S) = (\cos \theta_1, \dots, \cos \theta_m) \quad (2.20)$$

Distance metrics include projection, Binet-Cauchy, max correlation, min correlation, Procrustes, geodesic and mean distance [3], [18].

In general, metrics that rely on the smallest principal angle tend to be more robust to noise and less discriminative, while metrics that rely on the largest principal angle tend to be less robust to noise and more discriminative [19]. The distance between subspaces can also be calculated by converting the Grassmann manifold to an alternate space using Grassmann kernel. Projection kernels can be used to create an isometric embedding from Grassmann space to Hilbert space, which enables the use of Euclidean distance metrics. From [3], the projection kernel between subspaces  $x_1, x_2$  can be formed using

$$K_p(x_1, x_2) = \|x_1'x_2\|_F^2 \quad (2.21)$$

where  $\|\cdot\|_F$  is the Frobenius norm. Projection kernels do not define a direct linear relationship between subspaces and as a result kernel based methods such as PCA or LDA are needed for accurate classification [19].

Grassmann manifolds have been investigated for computer vision applications, such as object, action and face recognition. In [3] Hamm and Lee used Grassmann kernel LDA to increase performance in face and object recognition. Turaga et al. used

probability density functions to estimate classes on the Grassmann manifold in [4] and applied it to activity recognition, affine shape analysis and video based face recognition. In [18] Shigenaka et al. introduced GD-MSM and GK-SVM, which use the Grassmann manifold to improve the performance of mutual subspace method and support vector machines. In [19] Azary introduced Grassmannian Sparse Representations for 3D action and face recognition.

Table 1: Grassmann Distance Metrics

<i>Metric Name</i>	<i>Metric Equation</i>
Projection	$d_p(x_1, x_2) = \left( m - \sum_{i=1}^m \cos^2 \theta_i \right)^{\frac{1}{2}} \quad (2.22)$
Binet-Cauchy	$d_p(x_1, x_2) = \left( 1 - \prod_i \cos^2 \theta_i \right)^{\frac{1}{2}} \quad (2.23)$
Max Correlation	$d_p(x_1, x_2) = (1 - \cos^2 \theta_1)^{\frac{1}{2}} \quad (2.24)$
Min Correlation	$d_p(x_1, x_2) = (1 - \cos^2 \theta_m)^{\frac{1}{2}} \quad (2.25)$
Procrustes	$d_p(x_1, x_2) = 2 \left( \sum_{i=1}^m \sin^2 \frac{\theta_i}{2} \right)^{\frac{1}{2}} \quad (2.26)$
Geodesic	$d_p(x_1, x_2) = \sum_{i=1}^m \theta_i^2 \quad (2.27)$
Mean Distance	$d_p(x_1, x_2) = \frac{1}{m} \sum_{i=1}^m \sin^2 \theta_i \quad (2.28)$

## 2.4. LBP/LTP Features

Large variations in illumination are a challenging test case for many image based recognition techniques. One solution is to rely on descriptors based on texture rather than raw pixels. Local binary patterns (LBP) and local ternary patterns (LTP) summarize local grey-level structure and as a result are resistant to the effects of illumination. In [20], Ojala et al. introduced LBP for illumination invariant texture classification. In this technique a binary code is generated for each pixel in an image by comparing the center pixel to the neighboring pixels. The binary codes are given by the following

$$LBP = \sum_{i=0}^n 2^i s(y_i - y_c) \quad (2.29)$$

where  $y_c$  is the center pixel intensity,  $y_i$  is the pixel intensity in the surrounding neighborhood and  $s$  is given by

$$s(u) = \begin{cases} 1, & u \geq 0 \\ 0, & u < 0 \end{cases} \quad (2.30)$$

Originally the neighborhood was defined as the 3 x 3 area around the target pixel, however other patterns have been explored. Figure 5 highlights the encoding process using a 3 x 3 image patch.

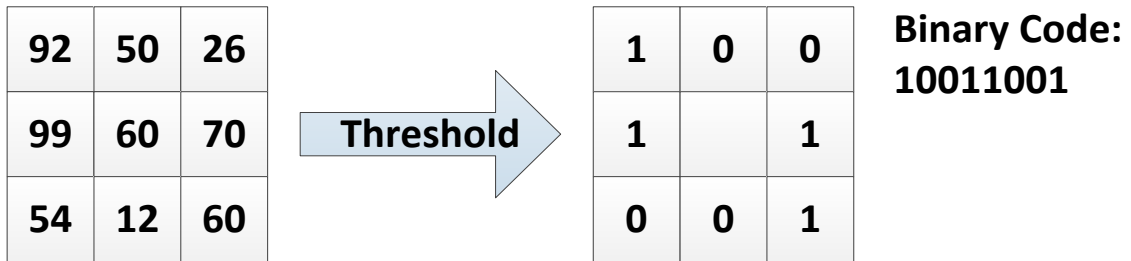


Figure 5: LBP Operator

LBP is highly discriminative on areas with uniform illumination, however areas with gradual illumination change introduce noise [21]. Tan et al. eliminate this issue by introducing LTP in [21], which replaces the threshold with a range and the binary code with a ternary code. Local ternary codes are given by the following

$$LTP = \sum_{i=0}^n 3^i s'(y_i - y_c, y_c, t) \quad (2.31)$$

where  $t$  is a user specified threshold and  $s'$  is given by

$$s'(u, y_c, t) = \begin{cases} 1, & u \geq y_c + t \\ 0, & y_c - t < u < y_c + t \\ -1, & u \leq y_c - t \end{cases} \quad (2.32)$$

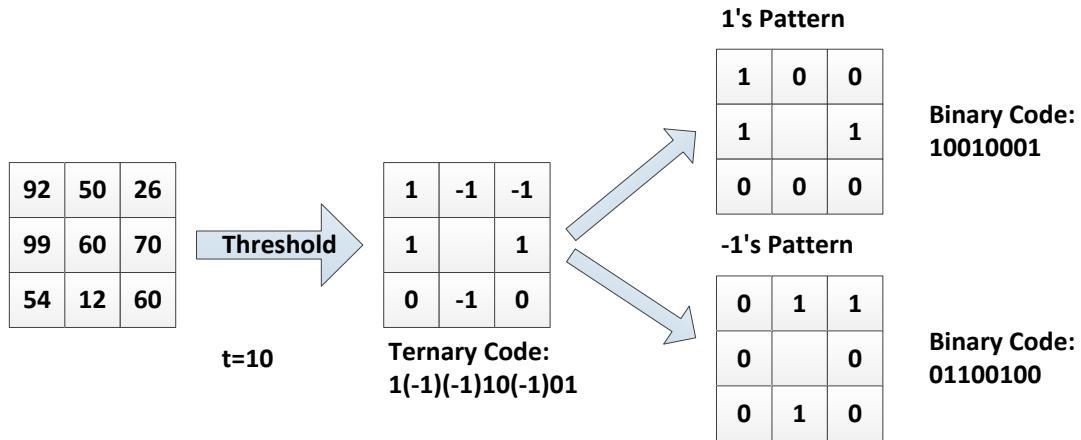


Figure 6: LTP Operator

For simplicity the ternary code is split into two binary codes and processed separately. Figure 6 shows this process for a 3 x 3 image patch. To perform recognition LBP/LTP is run on an image and local histograms are generated for image subsections. These

histograms are then concatenated to form a descriptor and recognition is performed using pattern recognition techniques.

## 2.5. GPU Acceleration

### 2.5.1 General Purpose GPU Computing

Originally GPUs were designed to reduce the computational load of the CPU by solely processing graphics request. In order to optimize graphics operations GPUs utilize a single instruction multiple data (SIMD) architecture, which simplifies control logic and utilizes a large number of simple arithmetic logic units (ALU) to take advantage of data level parallelism as shown in Figure 7.

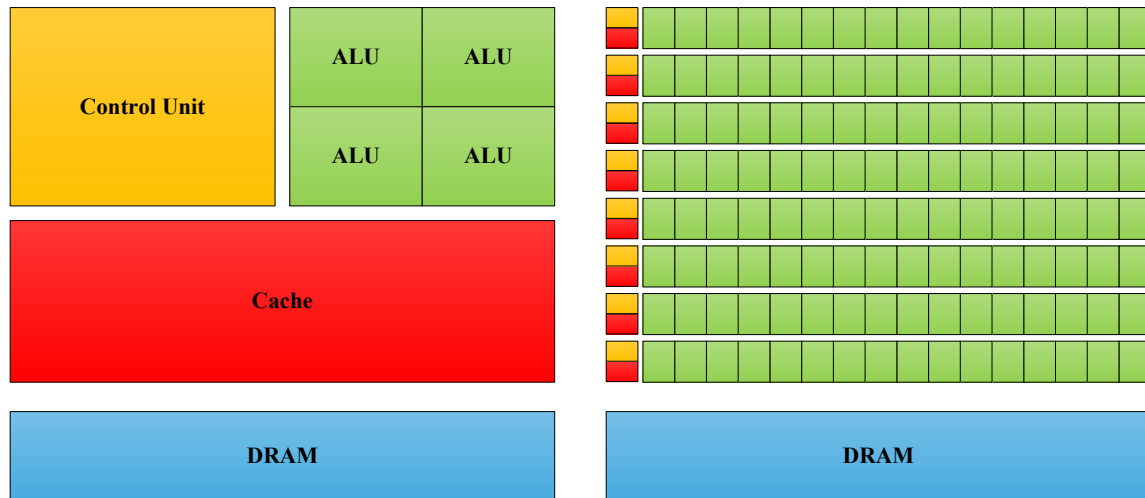


Figure 7: CPU Architecture (left) vs GPU Architecture (right)

In 2007, NVIDIA recognized the potential for heterogeneous CPU/GPU solutions and released the first general purpose computing on the GPU (GPGPU) API, the Compute

Unified Device Architecture (CUDA) [22]. CUDA and other GPGPU APIs have allowed researchers to speedup algorithms that were previously too computationally intensive for CPUs alone.

In order to maximize the performance of an algorithm on the GPU, the underlying hardware must be considered. CUDA-capable GPUs are organized into arrays of streaming multiprocessors (SM). Each streaming multiprocessor is composed of a set of streaming processors (SP) and connected to a shared block of DRAM called global memory. Each streaming processor shares control logic, an instruction cache, registers and another block of DRAM called shared memory. The number of streaming multiprocessors and streaming processors is important to consider when developing CUDA applications because they determine the maximum number of threads that can be run simultaneously. In CUDA threads are organized into 3D blocks which make up a 3D grid. The dimensionality of each of these 3D block/3D grid structures is application dependent. At runtime each streaming multiprocessor is assigned a block from the grid to execute. Each block is broken into groups of 32 threads called warps prior to execution. Each warp is then run in a serial manner over the streaming processors, this allows for fast context switching between warps when a stall is encountered.

Another important hardware consideration is memory usage, CUDA-capable GPUs allow the use of five different types of memory: registers, shared memory, global memory, constant memory, and texture memory. The bandwidth of the GPU's global memory is often a bottleneck in CUDA programs, therefore proper memory usage is important when developing high performance applications. Threads store local variables in registers and any overflow in a private section of global memory called local memory.

Registers are the fastest memory on the GPU, therefore it is important to limit the number of local variables for high performance applications. Shared memory is a read/write memory that allows memory sharing across threads in the same block. This is achieved by local DRAM blocks within each streaming multiprocessor. Overall this allows for much faster data storage without contributing to the global memory bandwidth. Global memory is a read/write memory that allows memory access by any thread. All incoming data and outgoing results must pass through global memory and as a result it is often the main bottleneck of the GPU. Another form of memory is constant memory which only allows read operations during runtime. Like global memory constant memory can be accessed by any thread, however it is highly cached making it much quicker than global memory. The final memory type is texture memory which is a special read only memory that has been optimized for texture based operations. Using special hardware built into the pipeline several common texture functions can be performed automatically including pixel interpolation and border wrapping. Unlike other forms of memory on the GPU, texture memory has constant access times for both cache hits and misses which allows for better scheduling and a 2D cache which gives it greater 2D spatial access.

There are several important design constraints to keep in mind when developing high performance algorithms in CUDA. Block size is very important design constraint in GPGPU because it controls how well your program hides memory latency. Generally block sizes are a fraction of the number of threads that a streaming multiprocessor can support so that multiple blocks can run on one streaming multiprocessor. The number of threads in a block should be a multiple of 32, to ensure that only full warps are generated. The number of conditional statements is another important factor to consider in high



performance applications. When a conditional branch statement is encountered in CUDA the diverging threads may need to be stalled until all threads converge. Therefore, to get good hardware utilization it is important to limit the number of conditional statements. As a result this reduces hardware utilization. One of the most important keys when working in CUDA is to be observant of the memory access patterns. In order to reduce overhead involved with accessing global memory each read has the potential to fetch 64 consecutive bytes. If memory is not coalesced it could take up to 16 reads to fetch the same number of bytes.

### **2.5.2 GPU accelerated $L_1$ -PCA**

There has been a lot of research on how to best utilize GPU resources to speedup algorithms. However, there has been very little research on how to specifically accelerate  $L_1$ -PCA using the GPU. In [2] Funatsu et al. accelerated Kwak's PCA- $L_1$  algorithm from [8] using the GPU. Funatsu et al. do not specify which portions of Kwak's PCA- $L_1$  algorithm they accelerated using the GPU. However, they do utilize CUBLAS, which is CUDAs optimized BLAS (Basic Linear Algebra Subprograms) library. Funatsu et al. report speedups between 1.72 – 2.96 over the CPU on small datasets [2].

## Chapter 3 L1-PCA Recognition

This chapter describes several approaches to recognition based on  $L_1$ -PCA. The design of the  $L_1$ -PCA algorithm is discussed in Section 3.1. In Section 3.2 the implementation of the  $L_1$ -Eigenfaces,  $L_1$ -Grassmann and LTP preprocessing is outlined. The CPU implementation of  $L_1$ -PCA is specified in Section 3.3. Lastly this chapter details the  $L_1$ -PCA GPU implementation in Section 3.4.

### 3.1. L1-PCA Algorithm Design

Recent work by Kundu et al. [12] introduced a fast computation for a single  $L_1$  principal component using bit flipping to maximize the  $L_1$  projection energy. The advantage of the Kundu et al. method is that the complexity is  $O(\tilde{N}N^2)$  where  $N$  is the number of samples and  $\tilde{N}$  is the number of initializations which are chosen by the user. Unlike previous solutions this method does not rely on the dimensionality of the data which makes it ideal for image recognition where the dimensionality is usually the number of pixels in the image. This method is extended to multiple components using the greedy search algorithm introduced by Kwak in [8]. Subsequent principal components are calculated by removing each principal components contribution from the data samples and utilizing the updated dataset to find the next principal component. This process is repeated until the desired number of components is reached. The greedy search algorithm guarantees that the principal components maximize the  $L_1$ -dispersion [8]. The overall algorithm flowchart is shown in Figure 8. The time complexity for the full algorithm is  $O(M\tilde{N}N^2)$  where  $M$  is the number of principal components.

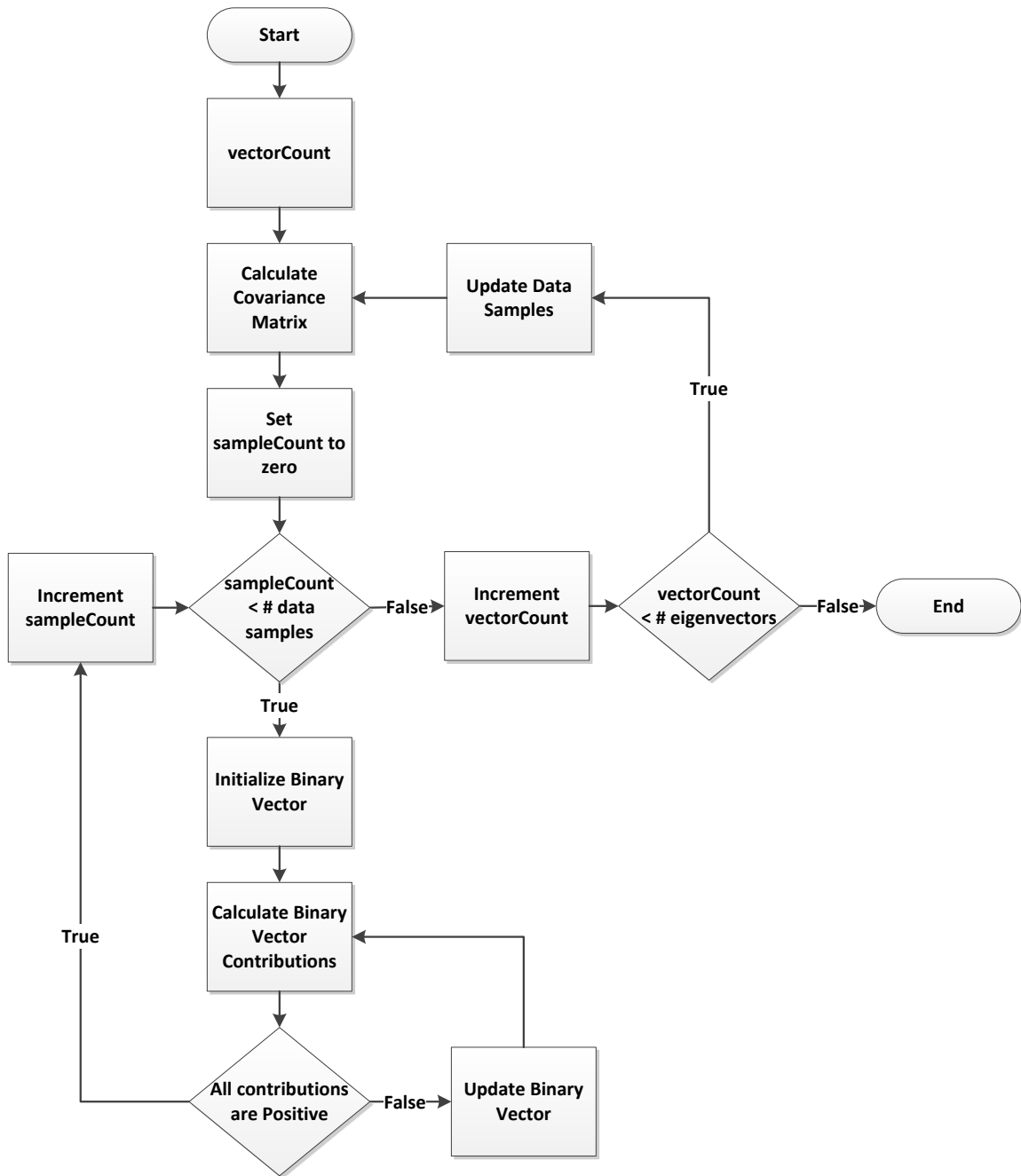
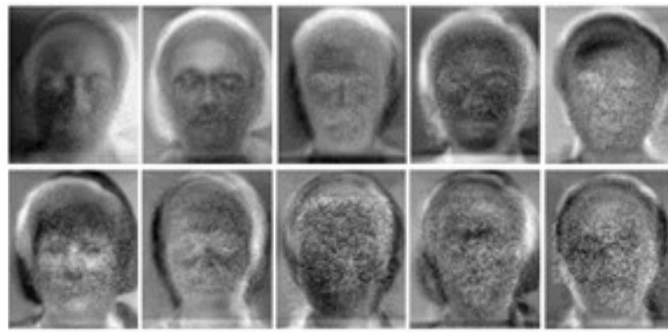


Figure 8: L1-PCA Algorithm Flow

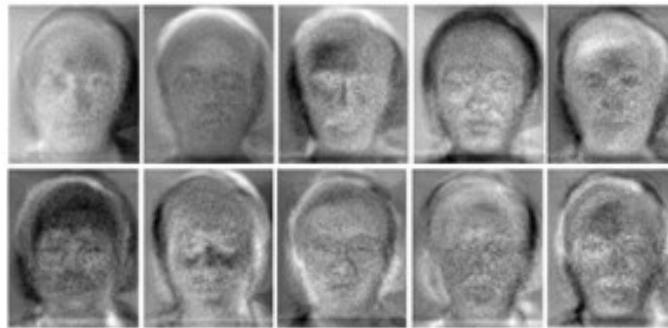
## 3.2. Recognition Techniques

### 3.2.1 L1-Eigenfaces

Much research has been performed to make eigenfaces more robust to variations in illumination and expression [23], [24], [25]. Utilizing the  $L_1$ -norm instead of the  $L_2$ -norm for eigenfaces allows for more accurate recognition on unconstrained or noisy datasets. Figure 9 shows the first ten eigenfaces generated from a subset of the aligned Yale Face database [25].



(a.)



(b.)

Figure 9: Eigenfaces from Occluded Dataset

The first 10 eigenfaces based on (a) L2-PCA and (b) L1-PCA from Yale Face Database.

Five images from each of the fifteen subjects were randomly chosen, then 30% of those images were partially occluded using rectangular noise.

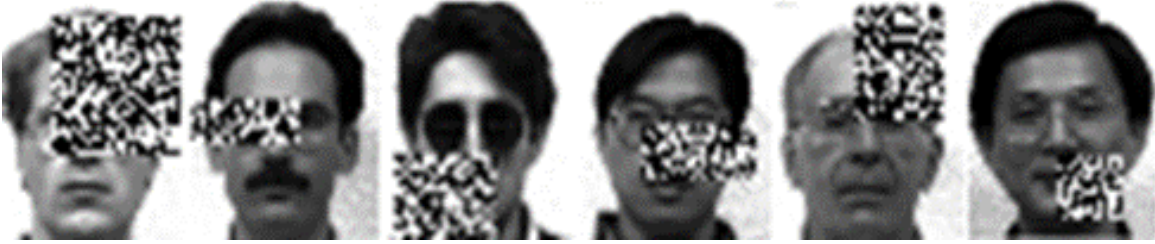


**Figure 10: Rectangular Noise on Yale Dataset**

The first eigenface is on the top left and the tenth is on the bottom right. We observe that the later eigenfaces capture more noise for both methods, however  $L_2$ -eigenfaces seem to degrade in quality much sooner as illustrated by eigenfaces 8, 9 and 10.

To perform recognition using  $L_1$ -eigenfaces the data matrix  $X = [x_1, \dots, x_N] \in R^{D \times N}$  needs to be formed such that columns are face image samples or LTP descriptors,  $D$  is the number of pixels or the length of the LTP descriptor and  $N$  is the number of samples. Without loss of generality, we can assume  $X$  is centered such that the set of samples  $\{x_i\}_{i=1}^N$  has zero mean. After that the  $L_1$ -PCA algorithm detailed in Figure 8 is used to calculate the  $L_1$ -eigenfaces. The greedy search in the  $L_1$ -PCA algorithm ensures that eigenfaces are presorted via their corresponding eigenvalues from largest to smallest. It is important to only use a subset of the eigenfaces because the later eigenfaces begin to capture noise. This subset of eigenfaces is used to transform training and test images into face space using the projection theorem. Once in face space a one nearest neighbor classifier is trained and used for face recognition. Nearest neighbor was chosen because it

is arguably one of the simplest classifiers and as a result it is better at highlighting the disparity between methods.

### 3.2.2 $L_1$ -Grassmann

Subspaces on the Grassmann manifold can be formed from a single data point or multiple data samples. As a result the Grassmann manifold can be used to make single-single, single-many or a many-many comparisons. To highlight the advantages of  $L_1$ -Grassmann we perform a many-many comparison where each subspace is composed of data samples from a single class. This doubles the effect of  $L_1$ -PCA by allowing it to reduce the effect of noise on both training and test images.

To construct  $L_1$ -Grassmann manifolds, first dictionaries are formed by sorting all training images or LTP descriptors and grouping them by the person's identity for face recognition or by expression for expression recognition. Each element in the dictionary is obtained by lexicographic ordering of all the image columns or by LTP preprocessing. Each class subspace is then mapped onto the  $L_1$ -Grassmann manifold by using the  $L_1$ -PCA algorithm detailed in Figure 8 to calculate the principle components for each class. After that the projection kernel is formed for the training and test set, which projects the manifold onto Hilbert space. Once in Hilbert space Grassmann PCA is used to reduce the dimensionality of the data and one-nearest neighbor classification is used for recognition. This entire process is shown below in Figure 11.

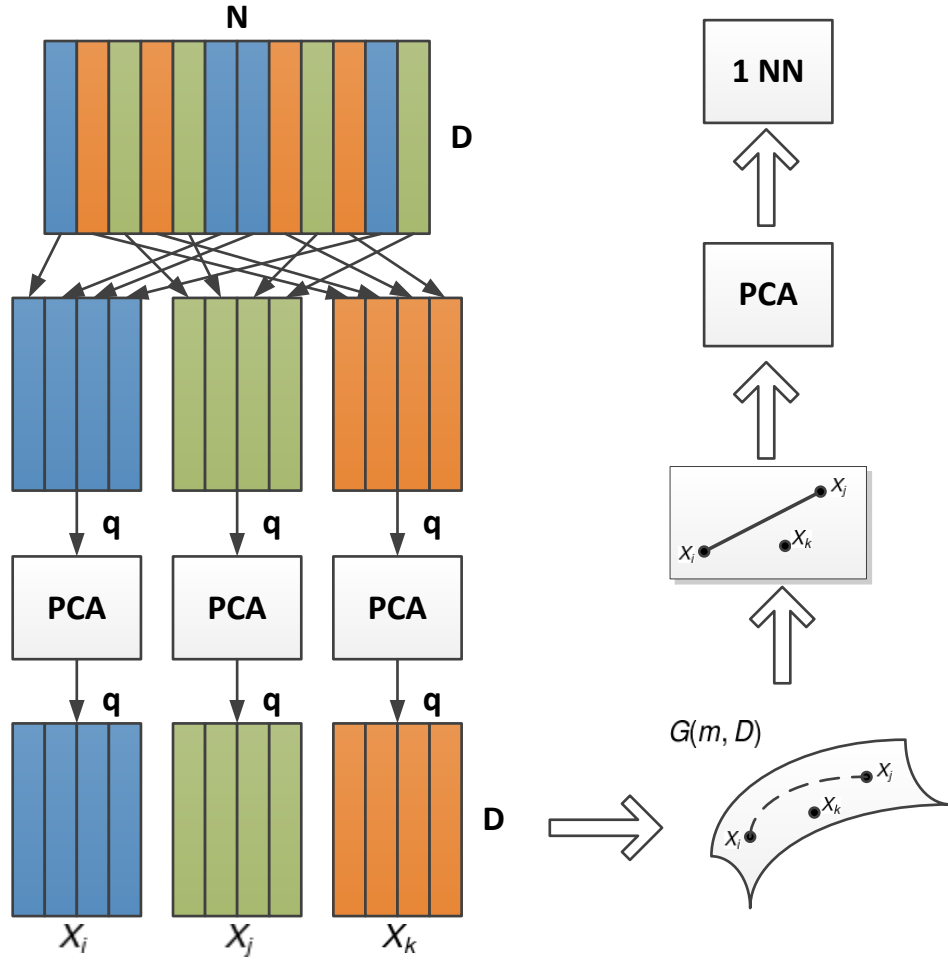


Figure 11: Recognition using Grassmann Manifolds

### 3.2.3 LTP Features

Local ternary patterns decode the grayscale structure in images and as a result can greatly improve accuracy in datasets with large variations in illumination. After performing LTP on an image traditional methods divide the LTP image into sub-regions and generate local histograms. These histograms are then concatenated together and used as a descriptor for the image. This technique reduces the dimensionality of the data by throwing away the spatial information within sub-regions. Since Eigenfaces and

Grassmann manifolds reduce the dimensionality of the data, it can be more advantageous to apply these techniques to the LTP image, instead of using LTP histograms. The overall procedure is to run LTP on each image in the dataset to produce an upper and lower coded image. After that both images are converted to vectors by a lexicographic ordering of all the image columns, this process is shown in Figure 12. Finally, these vectors are concatenated into a single descriptor and passed to Eigenfaces and Grassmann for recognition.

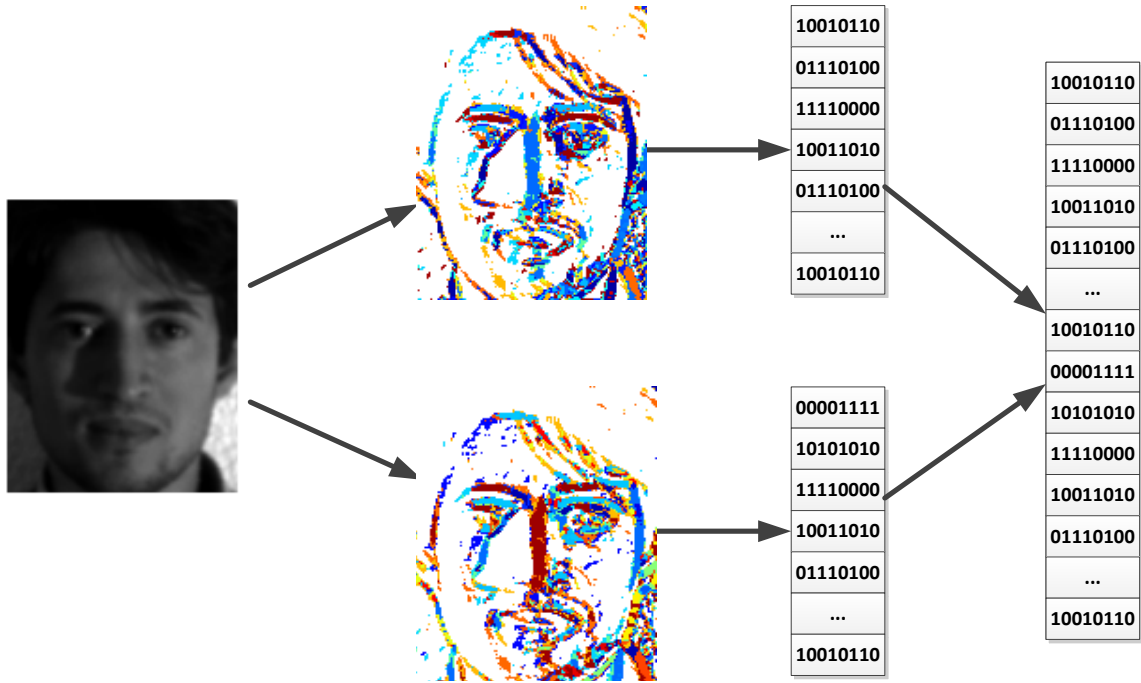


Figure 12: LTP Preprocessing

Each of the colors in the center images corresponds to a different LTP code

### 3.3. CPU Implementation

One way to accelerate the  $L_1$ -PCA algorithm is to take advantage of the parallelism of the algorithm and solve for the  $\tilde{N}$  potential eigenvectors in parallel. To



accomplish this the serial operations are vectorized and rewritten as a series of matrix operations. With this reformulation the goal becomes to optimize the binary matrix  $B \in \mathbb{R}^{\tilde{N} \times N}$  where each row corresponds to a potential eigenvector. The contributions of each bit in the binary matrix is solved simultaneously using

$$Q = B.* (B S_X) - D \quad (3.1)$$

where  $.*$  is element-wise multiplication and  $D \in \mathbb{R}^{\tilde{N} \times N}$  is

$$D = \begin{bmatrix} \text{diag}(S_X) \\ \vdots \\ \text{diag}(S_X) \end{bmatrix} \quad (3.2)$$

The binary matrix is updated by finding the minimum value in each row of  $Q$  and flipping the corresponding bits in the matrix  $B$ . To improve performance all minimum reductions are performed in parallel. This process is repeated until no bit in  $B$  contributes negatively or until the maximum number of iterations are reached. From the optimized matrix  $B$  the optimal binary vector is calculated by finding the row with the maximum projection energy. The following equation gives the projection energy for each row

$$E_p = \sum_{i=0}^N (B.* (B \times S_X))_{:,i} \quad (3.3)$$

where  $E_p \in \mathbb{R}^{\tilde{N} \times 1}$ . The optimal binary vector is then determined by performing a maximum reduction on  $E_p$  to find the largest corresponding projection energy. To ensure the optimal matrix operation performance the Intel Math Kernel Library which utilizes Basic Linear Algebra Subprograms (BLAS) was used to implement the algorithm for the CPU.

### 3.3.1.1 Reduction Algorithms

One of the most important areas to accelerate is the min and max reductions because of the large number of reductions used throughout the algorithm. The goal of a reduction algorithm is to perform an operation over a data vector and return a single value. This operation is often associative which allows it to be computed in a partially parallel manner. There are several reduction algorithms that are utilized throughout the  $L_1$ -PCA algorithm including the calculation of the minimum contributing bit and the calculation of optimal binary vector. To ensure high performance Intel's `parallel_reduce` function from the threading building blocks library was used. To maximize the parallelism in reduction algorithms this function generates a tree structure by recursively splitting the data vector into subranges until each subrange is no longer divisible as shown in Figure 13.

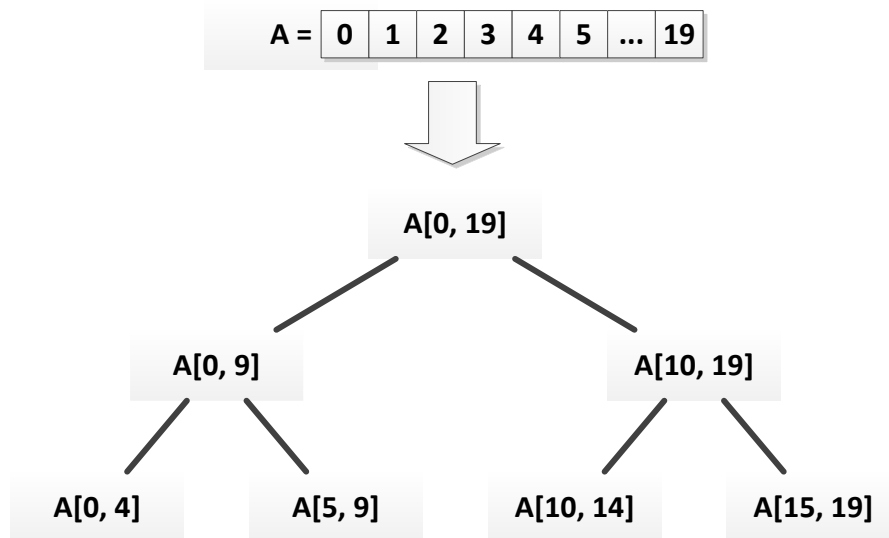


Figure 13: CPU Tree Reduction

Each node performs the desired operation such as max or min over its range and passes the result to the parent node. After that the parent node repeats this operation on the resultant of the child nodes. This process repeats until a single result is obtained through the root. This structure enables nodes at the same depth to be run in parallel and as a result accelerates the operation.

### **3.3.1.2 Parallel Operations**

Some of the matrix operations such as binary matrix initialization and optimization can be implemented more efficiently using custom parallel functions instead of BLAS functions. To ensure optimal performance Intel's `parallel_for` function was used for the custom functions. In a similar manner to the reduction algorithm the data vectors are recursively split into subranges until each subrange is no longer divisible. However in this case each subrange is independent and as a result only the leaf nodes need to be executed. Upon execution each element in a nodes subrange is executed in a synchronous fashion, however each node is executed in parallel. This methodology ensures that each thread is performing enough work to hide the latency involved in launching the extra threads.

## **3.4. GPU Implementation**

For the GPU implementation the vectorized  $L_1$ -PCA algorithm discussed in the CPU section was adapted for the GPU. The algorithm was broken into several smaller kernels. These smaller kernels allow greater thread control which reduces warp splitting and in turn produces higher hardware utilization. Large kernels use more registers and

can force the compiler to utilize Global memory for local variables. The main disadvantage is the additional time needed to launch each kernel, however the extra launch latency is made up by the better hardware utilization.

To ensure the high performance CUBLAS is used to perform matrix operations on the GPU. However, several high performance custom kernels were developed to handle the operations not supported by CUBLAS including sign, calcBitContribution, bitFlip, elementMultiply, scaleVector, vectorSubtraction, minReduction, maxReduction and sumReduction. The sign kernel is used to initialize the binary matrix  $B$  by calculating the sign of each element in the covariance matrix in parallel. Positive elements in the covariance matrix are initialized as +1 and negative elements as initialized as -1. The calcBitContribution kernel is used to determine how each bit in a vector contributes toward projection energy, it performs the following operation

$$f(X, B, S_x) = B.*X-D \quad (3.4)$$

To reduce the effects of the non-coalesced reads associated with the diagonal of  $S_x$ , the diagonal is read once into shared memory, instead of  $N$  times into local memory. After that each thread performs the multiplication and subtraction of a single element in parallel. The bitFlip kernel is passed the minimum bit contribution for each eigenvector and its index location. Then using a ternary operator to avoid warp splitting it flips the bits in the  $B$  matrix. The elementMultiply kernel is used when computing the projection energy to find the optimal eigenvector and performs element-wise multiplication using a single thread for each element.

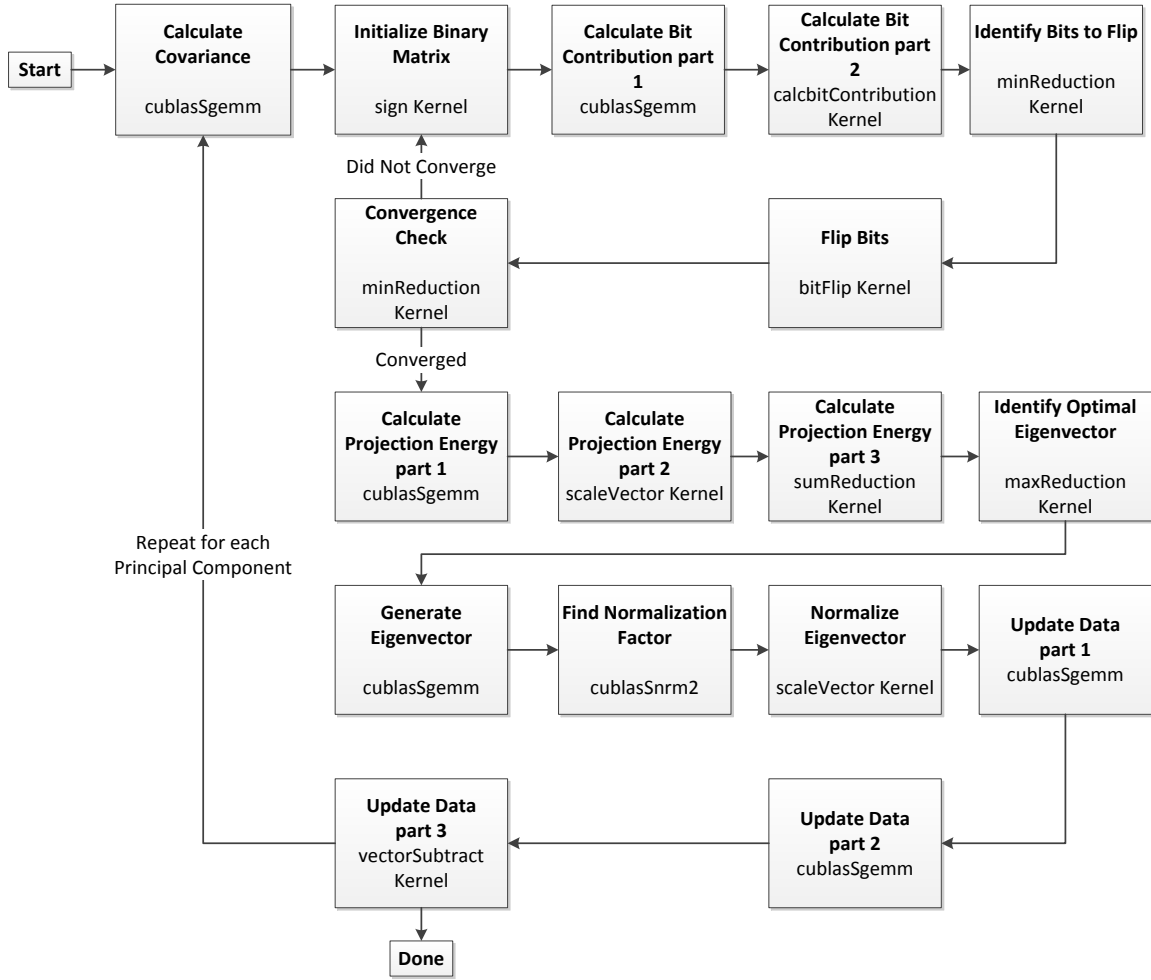


Figure 14: GPU Kernel Flow

The scaleVector kernel applies a scalar value to each element in a vector and is used to normalize eigenvectors. The vectorSubtraction kernel is used to update the data samples in the greedy search and performs vector subtraction between two vectors or matrices. Both scaleVector and vectorSubtraction operate using threads for each element in the vector. The three reduction kernels are designed so that they can compute a single reduction for a vector or a reduction for each row of a matrix. They are used several times throughout the algorithm and as a result have been highly optimized, the specifics can be

found in Section 3.4.1.1. The rest of the operations are performed by CUBLAS to ensure high performance, the GPU kernel flow is depicted in Figure 14.

### 3.4.1.1 Reduction Algorithms

Reduction algorithms are challenging to optimize on the GPU because the number of threads is reduced with each iteration which results in warp splitting. Furthermore the reduction operation cannot guarantee coalesced memory access, which greatly hurts performance. To address these issues a high performance reduction algorithm was developed for the GPU implementation. First the data vector is divided into power of two sized blocks, this ensures that operations are reduced by half every reduction cycle.

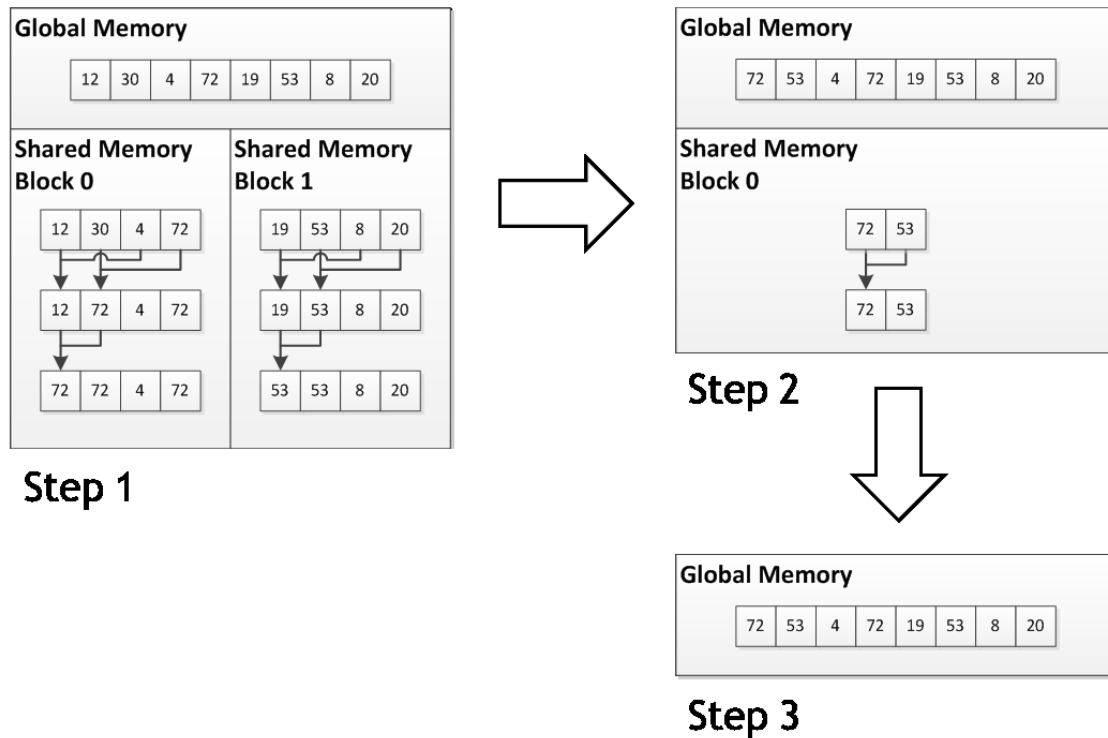


Figure 15: GPU Reduction

After that data is loaded into shared memory, this is done to reduce memory latency and alleviate non-coalesced memory problems. Next a reduction cycle is run to reduce the number of operations in half. A reduction cycle consists of threads equal in number to half the data performing the desired operation such as max or min. The lower indexed values and the high indexed values are used as operands to ensure that only coalesced memory operations occur. The result is then saved in the lower indexed values of shared memory and the data count is reduced by half. If more than one block is needed the process is repeated with a new kernel, this is done to ensure synchronization across blocks and to maintain hardware utilization. This entire process is depicted in Figure 15 and pseudo code is provided in Figure 16. One advantage of this algorithm is that it can be easily extended to perform multiple reductions on a single matrix in parallel by simply increasing the number of blocks used to perform reduction.

```
// Global Variables
// floatMax- the maximum float value
// TILE_SIZE- the number of threads in a 1D block
__global__ void minReduction(float* dIn, int size, float* dOut){
    __shared__ float shared[TILE_SIZE]; // initialize shared memory
    int dataID = blockIdx.x * blockDim.x + threadIdx.x; // Global memory index
    int length = TILE_SIZE; // Number of comparisons for current reduction(power 2)

    // load data into shared memory
    shared[threadIdx.x] = (dataID < size) ?
        dIn[(blockIdx.y*size) + dataID] : floatMax;
    __syncthreads();

    // perform reduction
    while(length > 1){
        length = length /2;
        if(threadIdx.x < length){
            shared[threadIdx.x] = (shared[threadIdx.x + length] < shared[threadIdx.x]) ?
                shared[threadIdx.x + length] : shared[threadIdx.x];
        }
        __syncthreads();
    }

    // write output
    if(threadIdx.x == 0){
        dOut[(blockIdx.y*gridDim.x)+blockIdx.x] = sharedArray[0];
    }
}
```

**Figure 16: Min Reduction Kernel**

## **Chapter 4    Experimental Results**

### **4.1.   *Experimental Setup***

For each experiment, the images are converted to greyscale and resized to a final resolution of  $100 \times 90$  pixels before performing recognition. Several experiments are run on occluded versions of various datasets. These datasets are generated by adding rectangular noise occlusions to 30% of the images in the database. The location of the rectangular noise is determined randomly, and its size is randomly chosen between  $15 \times 15$  and  $60 \times 60$ . The noise in the rectangular window consists of normally distributed white and black pixels.

Eigenface experiments use each test image for single to single classification and record the average accuracy for a varying number of eigenvectors. For Grassmann manifold experiments all test images are sorted into their designated class for many to many classification and the average accuracy for a varying number of Grassmann eigenvectors is recorded. Each experiments consist of two separate trials of 4-fold cross validation unless stated otherwise. The accuracies reported are the average accuracies across both trials.

### **4.2.   *Datasets***

#### **4.2.1 Yale Face Database**

The Yale Face database contains 165 grayscale images of 15 different people [25]. There are 11 images for each subject and they vary in illumination and facial expression. Image configuration include centered light, left light, right light, glasses on,



glasses off, neutral expression, sad, sleepy, wink and surprised. To improve face recognition accuracy a normalized version of the Yale Face database is used where faces are rotated, cropped and centered such that the eyes of each subject are aligned [26].



**Figure 17: Yale Face Database Images Across Two Subjects**



**Figure 18: Yale Face Database Sample Image from each Subject**

### 4.2.2 AT&T Database of Faces

This AT&T Database of Faces formerly known as the ORL face database contains 400 images of 40 different people [27]. There are 10 images for each subject and they vary in pose and facial details such as glasses. Images were taken over time and as a result minor lighting changes occur across subjects.



Figure 19: AT&T Database Images Across Two Subjects



Figure 20: AT&T Database Sample Image from each Subject

### 4.2.3 Extended Yale Face Database B

The Extended Yale Face Database B contains 2,432 images of 38 different people [28]. There are 64 images for each subject and they vary in illumination. Face images vary greatly in illumination across subjects, so much so that at times only a small portion of the face is visible. To improve face recognition accuracy a close cropped version of the dataset is used, where each image is cropped to include only the face with no background or hair.

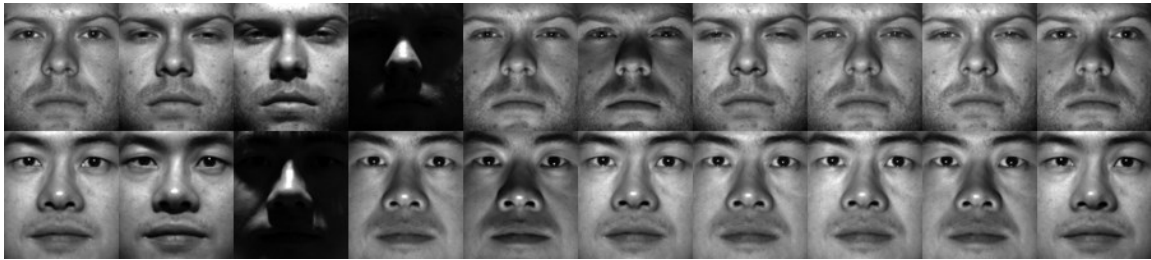


Figure 21: Extended Yale Face Database B Images Across Two Subjects



Figure 22: Extended Yale Face Database B Sample Image from each Subject

#### 4.2.4 AR Face Database

The AR Face Database contains 2,600 color images of 100 different people, 50 men and 50 women [29]. There are 26 images for each subject and they vary in expression, illumination and natural occlusions. Subjects in this dataset utilize scarfs or large sun glasses to occlude parts of their face making recognition difficult.



Figure 23: AR Face Database Sample Image from each Subject



**Figure 24: AR Face Database Images Across a Subject**

#### **4.2.5 Labeled Faces in the Wild Database**

The Labeled Faces in the Wild database contains 13,233 images of 5749 different people [30]. Unlike the other database the number of images per subject varies and only 1680 subjects have two or more images. The dataset was generated by running the Viola-Jones face detector [31] on a large database of images and scaling up the resulting area to include the background. The LFW face database is a challenging dataset because many forms of variation are present including variations in pose, lighting, expression, background, race, ethnicity, age, gender, clothing, hairstyles, camera quality, color saturation and focus [30]. To improve face recognition accuracy a deep funneled version of the database is used such that each image is aligned [32].



**Figure 25: LFW Face Database Images Across Two Subjects**



Figure 26: : LFW Face Database Subjects with at Least 20 Images

#### 4.2.6 Cohn-Kanade Databases

The Cohn-Kanade database contains 97 subjects in 228 expression sequences [33]. The extended Cohn-Kanade database is an expansion of the original Cohn-Kanade database and contains 118 subjects in 327 expression sequences [34]. Each sequence varies in the length and begins with a neutral expression and transitions into 1 of 7 expressions including anger, contempt, disgust, fear, happy, sadness and surprise. To improve recognition accuracy each image is cropped to the face using the landmark points provided.



Figure 27: Emotions from the Extended Cohn-Kanade Database

From left to right anger, disgust, fear, happy, sadness, and surprise (©Jeffrey Cohn)

### 4.3. *Parameter Selection*

The maximum number of iterations is used to terminate the eigenvector optimization process if the algorithm does not converge. The number of iterations required to optimize the eigenvector is a function of the number of data samples. To ensure that each binary vector is properly optimized  $3N$  iterations are used. This ensures that each bit has the chance to be flipped at least three times. In practice most binary vectors converge in  $\sim 2N$  iterations.

Another important parameter is  $t$  which is used to determine the upper and lower boundaries in the local ternary patterns feature extraction, as shown in (2.32). The variable  $t$  controls how much of the grayscale structure is considered noise. If  $t$  is too low, then LTP captures the noise in smooth areas, however if  $t$  is too large LTP does not capture some of the weaker textures. Some work has been done on picking optimal  $t$  values. In [35] a data adaptive approach was developed that uses Weber's Law and the central pixel to set  $t$ . However, their work was not tested on datasets with variations in illuminations. In [21] LTP was run extended Yale B and several other datasets with large variations in illuminations and they found  $t = 5$  is a good threshold for removing illumination effects. To find the optimal LTP threshold each experiment is repeated for  $t = [1, 20]$  and the optimal value and its corresponding threshold are reported.

Two parameters that greatly affect the performance of the GPU algorithm are the main block size and reduction block size. The block size is the number of threads used in a single CUDA block, to get full GPU utilization the number of threads across all blocks should be a multiple of 32 so that only full warps are generated. The main block size is used for all the custom CUDA kernels except for the reduction kernels, which use the

reduction block size. The reduction block size has additional constraint; it should be a power of two so that a full reduction can be performed every reduction cycle. Two GPUs are used throughout experiments the GeForce GTX 480 and Tesla K20c. The GeForce GTX 480 can support at maximum 1024 threads per blocks and 1536 threads per multiprocessor. The optimal main and reduction block size for the GeForce GTX 480 are 768 and 512. The Tesla K20c can support at maximum 1024 threads per blocks and 2048 threads per multiprocessor. The optimal main and reduction block size for the Tesla K20c are 1024 and 1024.

#### **4.4. Accuracy Tests**

In the first two experiments, recognition accuracy was collected from the Yale, AT&T and extended Yale databases. All data was normalized and centered such that the mean was zero and the standard deviation was one. Results were collected using a variant of four fold cross validation that ensured the number of images of a person was the same for each fold. In the first experiment the  $L_1$ -eigenfaces and  $L_1$ -Grassmann face recognition techniques are compared against the  $L_2$  versions on the original databases. This test ensures that the suboptimal methods utilized to accelerate  $L_1$ -PCA do not negatively affect the recognition accuracy. Twenty five iterations of 4 fold cross validation was used to establish a baseline for the eigenface comparison.



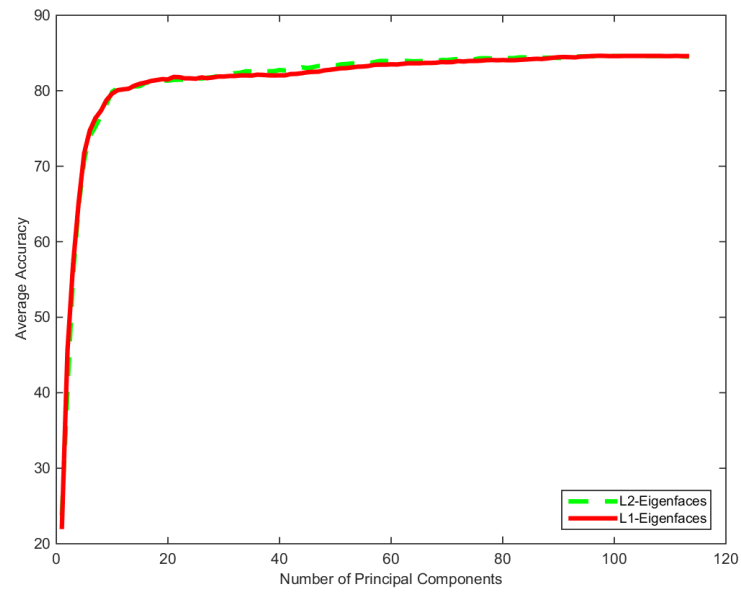


**Figure 28: Eigenface Comparison Test Yale Database**

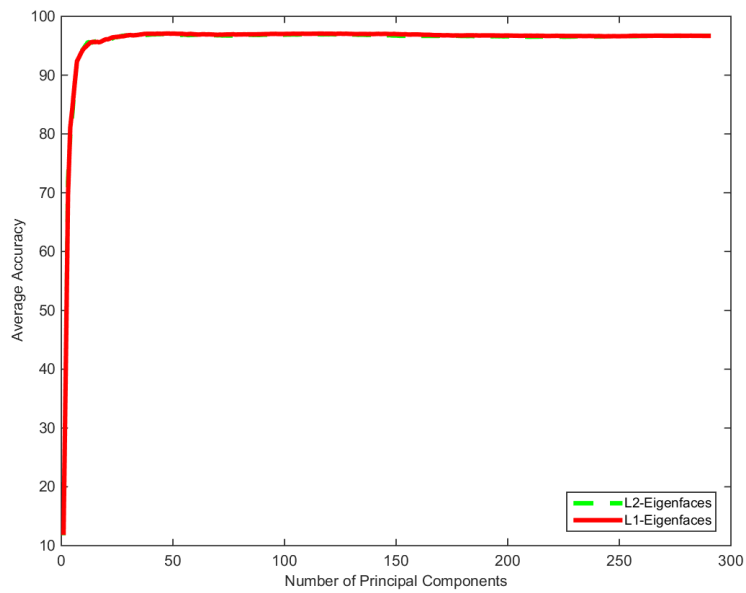


**Figure 29: Eigenface Comparison Test AT&T Database**

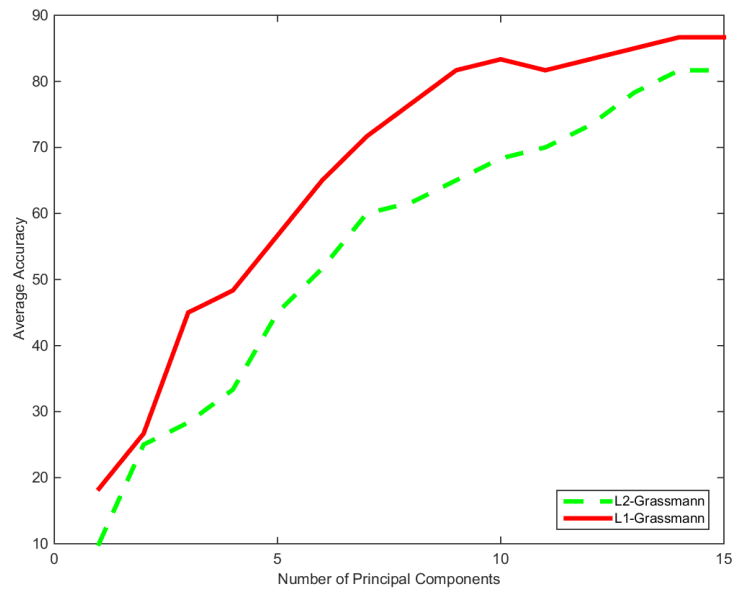


**Figure 30: Grassmann Comparison Test Yale Database**

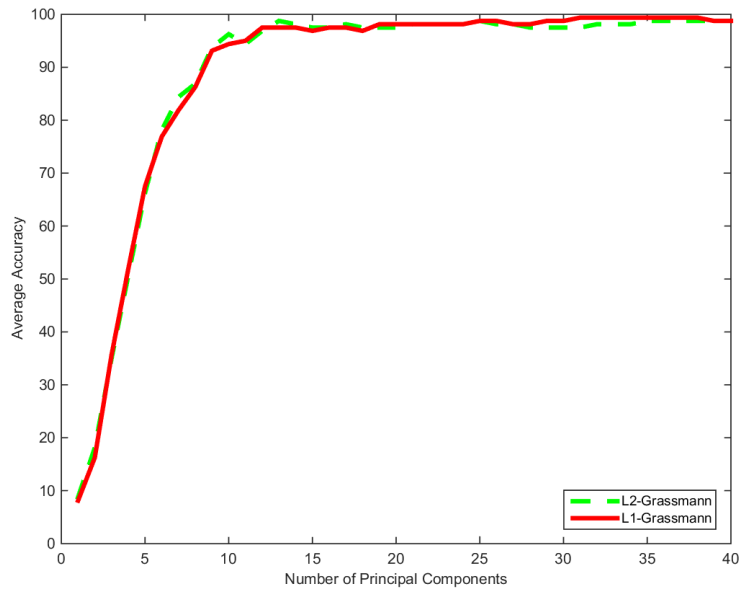


**Figure 31: Grassmann Comparison Test AT&T Database**

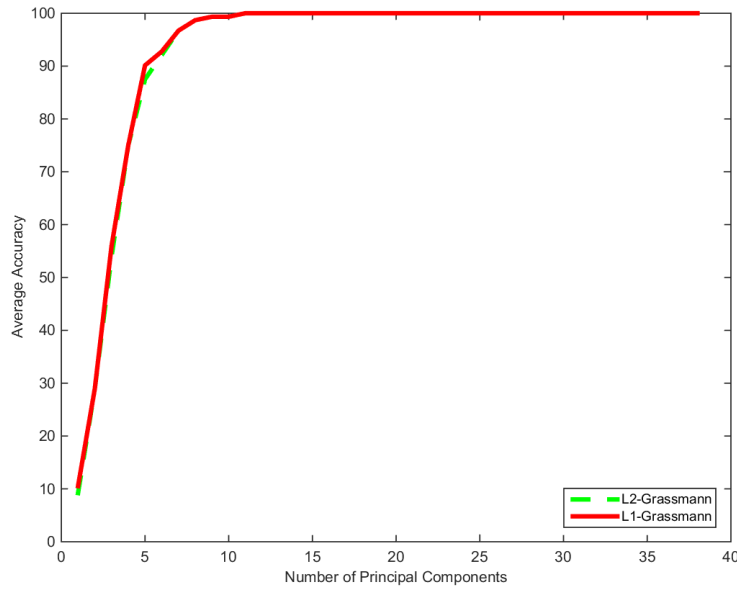


**Figure 32: Grassmann Comparison Test Extended Yale B Database**

All of the  $L_1$ -PCA based techniques performed as good as or better than the  $L_2$ -PCA based techniques indicating that the suboptimal methods utilized by  $L_1$ -PCA did not negatively affect recognition performance. Furthermore  $L_1$ -Grassmann outperformed  $L_2$ -Grassmann by  $\sim 10\%$  on the Yale database Figure 30. The Yale database has the fewer images per subject than any other databases tested, as a result when the Grassmann manifold is being formed noise has a greater influence.  $L_1$ -PCA was able to mitigate the effect of the noise and as a result improve recognition for  $L_1$ -Grassmann.

In the second experiment rectangular occlusions are added to 30% of all images in each database and the procedure from the first experiment is repeated on the occluded datasets. This experiment highlights the effectiveness of  $L_1$ -PCA at reducing the impact of noise in face recognition techniques. Once again  $L_1$ -Eigenfaces was run for 25 iterations of 4 fold cross validation.

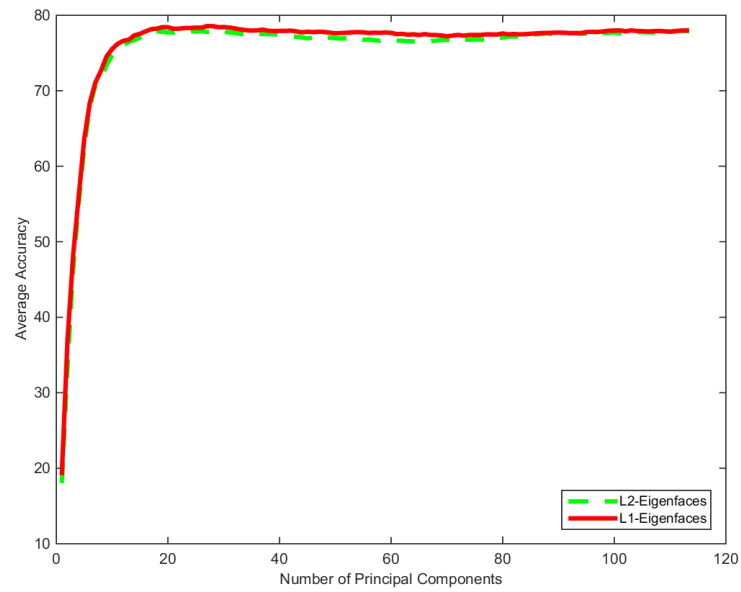


**Figure 33: Eigenfaces Comparison Test Occluded Yale Database**

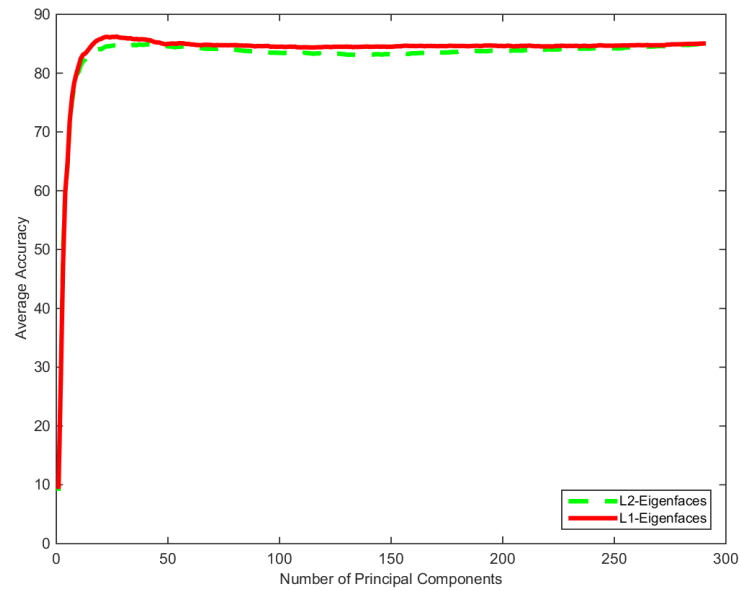


**Figure 34: Eigenfaces Comparison Test Occluded AT&T Database**

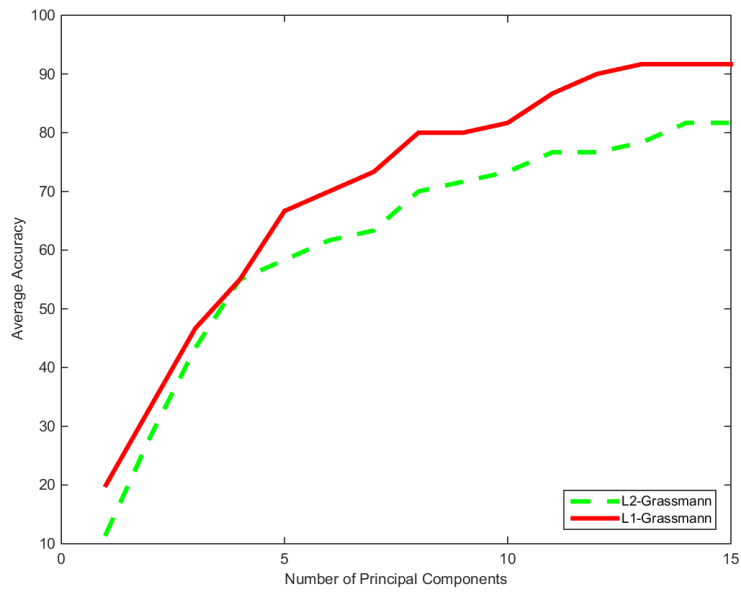


**Figure 35: Grassmann Comparison Test Occluded Yale Database**

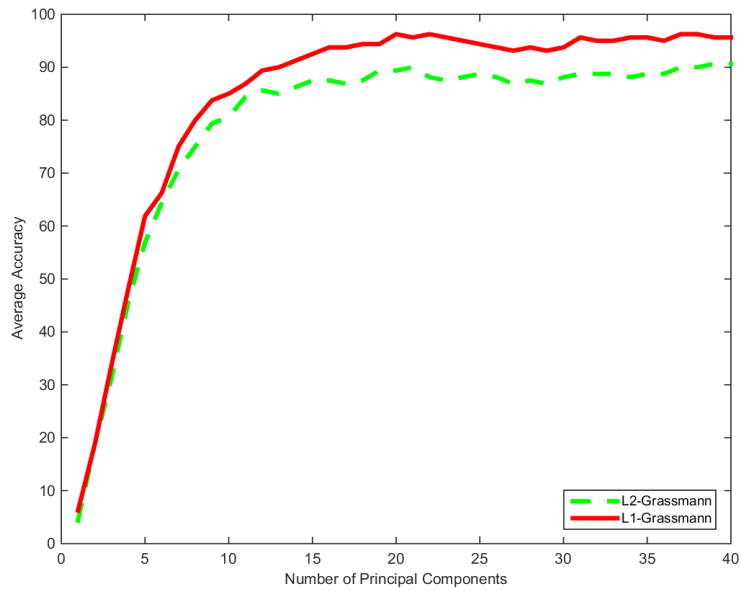


**Figure 36: Grassmann Comparison Test Occluded AT&T Database**

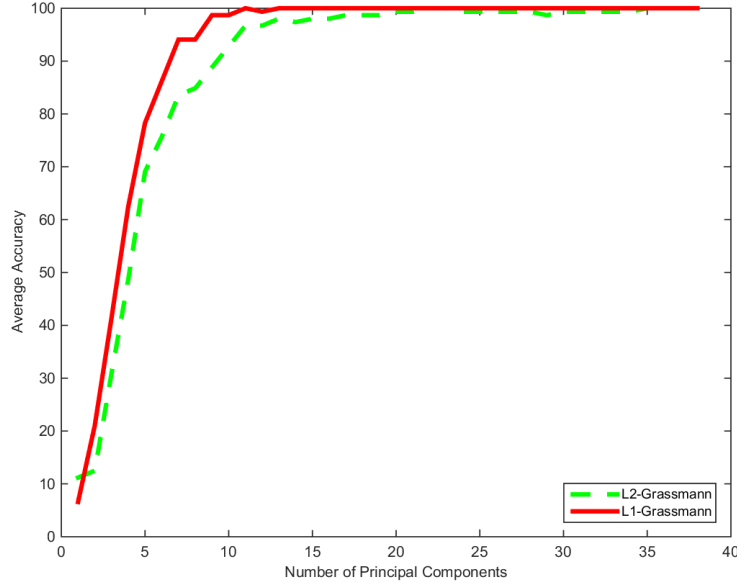


**Figure 37: Grassmann Comparison Test Occluded Extended Yale**

The  $L_1$ -PCA based techniques outperformed all of the  $L_2$ -PCA based techniques indicating that  $L_1$ -PCA is more robust to noise. Across both dataset  $L_1$ -Eigenfaces performed around 1-2% better than traditional eigenfaces.  $L_1$ -Grassmann did significantly better and outperformed  $L_2$ -Grassmann by  $\sim 10\%$  on the Yale database Figure 35 and around 5% better on the AT&T database Figure 36. Additionally  $L_1$ -Grassmann was able to reach 100% accuracy with 22 fewer eigenvectors than  $L_2$ -Grassmann on the Extended Yale B database Figure 37.

In the third experiment LTP preprocessing was tested by comparing the recognition accuracy across different values of  $t$  for  $L_2$ -Eigenfaces and  $L_1$ -Eigenfaces on the Yale database. This test explores how different values of  $t$  affect recognition accuracy on a dataset with illumination variation.

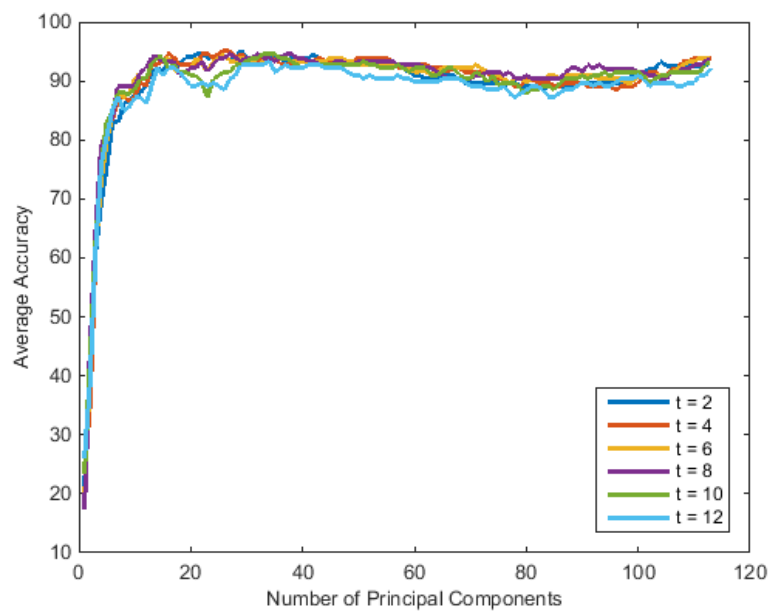


**Figure 38: LTP L2-Eigenface  $t$  Test for Yale Database**

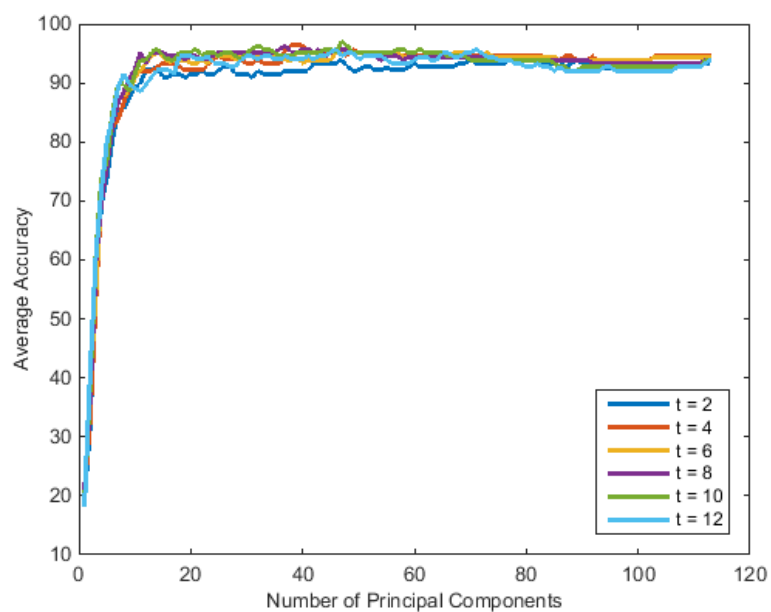


**Figure 39: LTP L1-Eigenface  $t$  Test for Yale Database**

This experiment shows that the actual  $t$  value chosen for LTP does not have a significant impact on recognition performance. The results for  $L_2$ -Eigenfaces in Figure 38 show that accuracy varies on average by  $\sim 3\%$  between  $t$  values. The results for  $L_1$ -Eigenfaces in Figure 39 show that accuracy varies on average by  $\sim 3\%$  between  $t$  values. In general, a  $t$  value of 2 is recommended for face recognition because it produces good recognition results across the Yale, AT&T and extended Yale database for LTP  $L_2$ -Eigenfaces.

In the fourth experiment LTP preprocessing was tested by comparing the accuracy results between the different face recognition techniques. The  $t$  value with the maximum recognition accuracy is reported for each test. This experiment highlights the effectiveness of LTP at removing the effect of illumination variation from Eigenfaces and Grassmann face recognition.

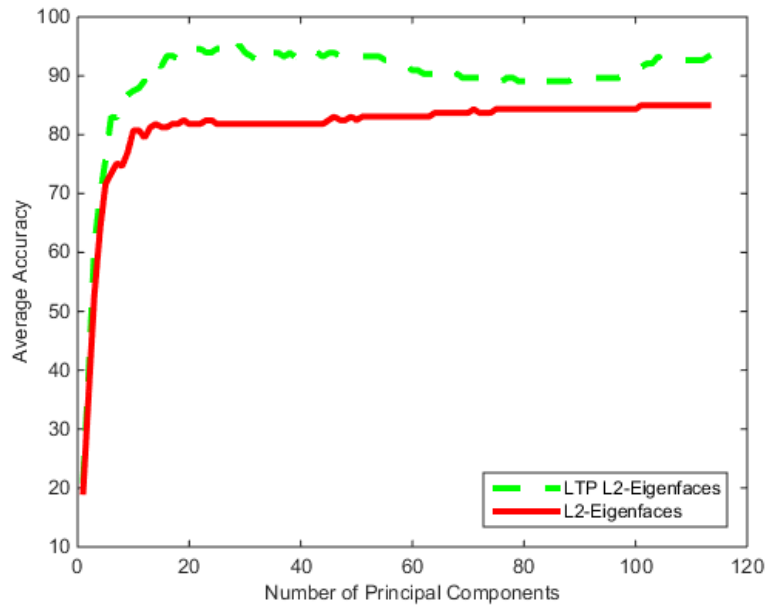


Figure 40: LTP Eigenfaces Test Yale Database ( $t = 2$ )



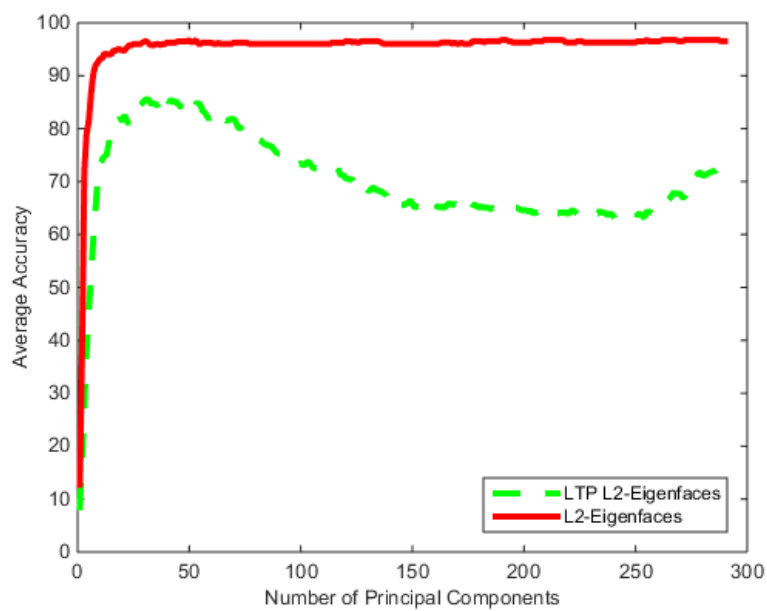


Figure 41: LTP Eigenfaces Test AT&T Database ( $t = 6$ )

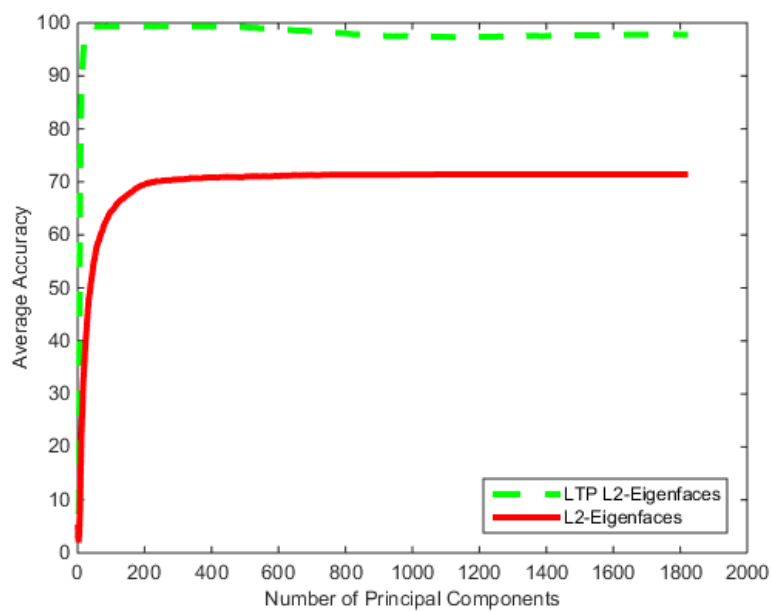


Figure 42: LTP Eigenfaces Test Extended Yale B Database ( $t = 1$ )

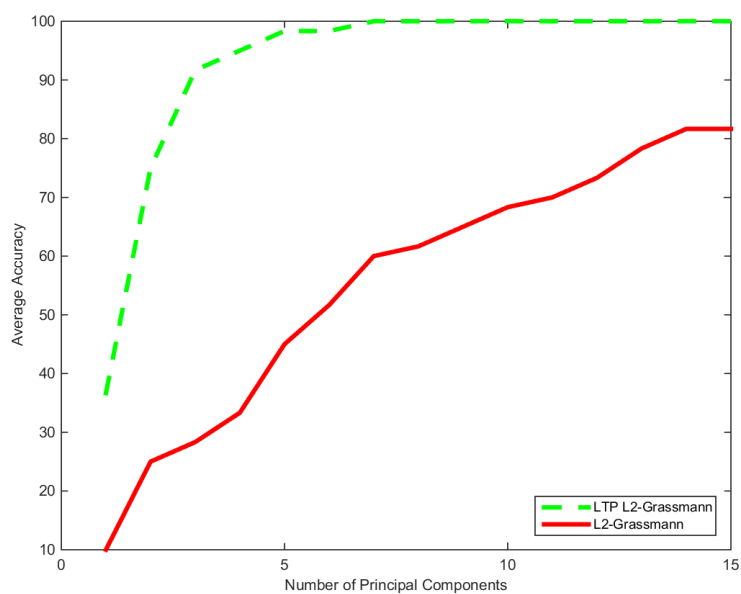


Figure 43: LTP Grassmann Test Yale Database ( $t = 5$ )

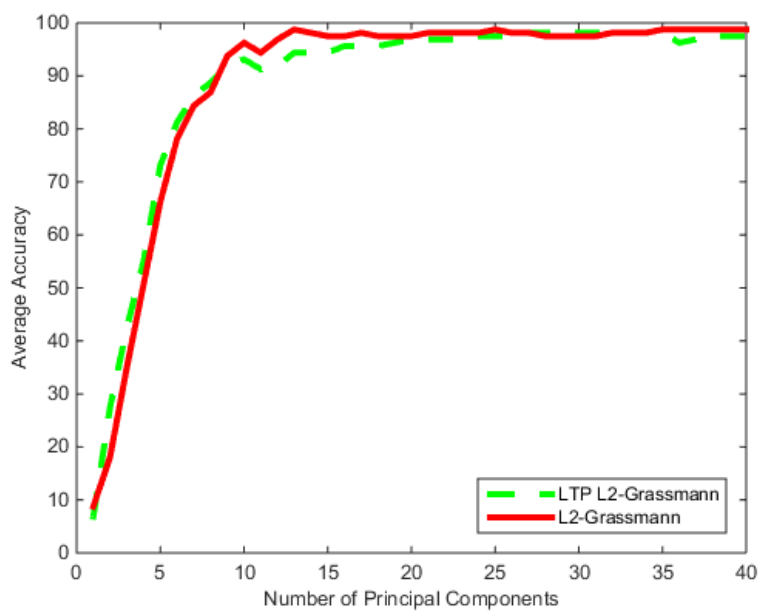
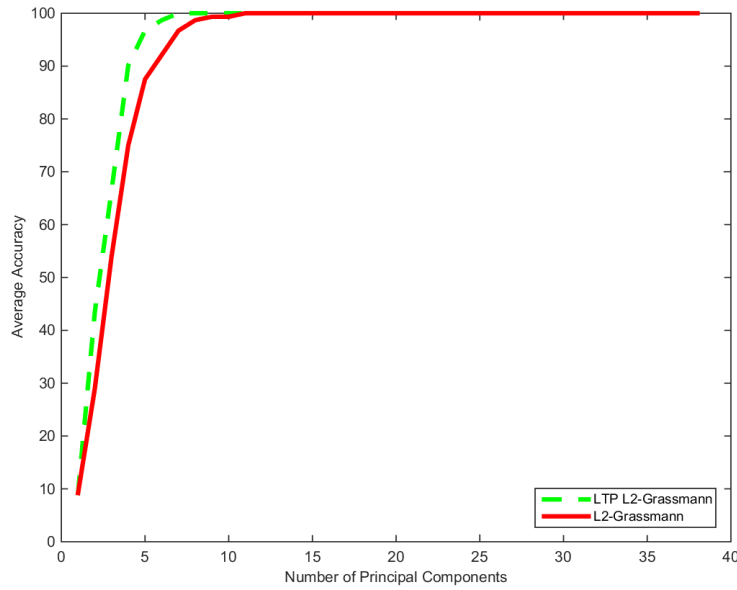


Figure 44: LTP Grassmann Test AT&T Database ( $t = 6$ )



**Figure 45: LTP Grassmann Test Extended Yale B Database (t = 5)**

LTP with  $L_2$ -Eigenfaces outperformed traditional  $L_2$ -Eigenfaces (without LTP) by about ~15% on both Yale Figure 40 and the Extended Yale database Figure 42. However, they performed significantly worse on the AT&T database Figure 41. LTP characterizes the underlying greyscale structure which allows it to perform well on datasets with great variation in illumination. However, when LTP is used to preprocess images it throws away the actual intensity values of the pixels which can be useful for recognition if the dataset of the underlying grey level structure is apparent. Since the AT&T database does not contain a significant amount of variation in illumination the traditional  $L_2$ -Eigenfaces works better because it has more information to work with.

Another major feature of the results is that the recognition accuracy degrades after a certain number of principal components. LTP preprocessing has a larger dimensionality because its feature vector is a concatenation of the upper and lower images and as a result

we approach a special case for principal component analysis where we have data that has large dimensionality and few samples. In [36] this special usage case is explored and they find that if the first few principal components capture most of the variance, then the other principal components will not converge to the appropriate subspace. As a result it is advisable to choose only a modest number of principal components to maximize recognition accuracy when using LTP preprocessing.

The LTP  $L_2$ -Grassmann also outperformed traditional  $L_2$ -Grassmann, on the Yale database LTP was  $\sim 18\%$  better Figure 43 and on the Extended Yale B database Figure 45 it converged to 100% accuracy with 5 fewer principal components. Once again LTP was outperformed on the AT&T database Figure 44, due to the missing information.

In the fifth experiment LTP  $L_1$ -Grassmann and LTP  $L_2$ -Grassmann is run on the Yale, AT&T, Extended Yale B, AR, LFW, Cohn-Kanade and Extended Cohn-Kanade databases. For the expression recognition experiments only happy, sadness, surprise and anger are used, while disgust and fear were ignored. To ensure accurate results the average accuracy from ten iterations of ten-fold cross validation are reported for expression recognition. This test is meant to evaluate the optimal performance of these recognition methods on challenging datasets.

Across all of the databases, LTP  $L_1$ -Grassmann performed as good as or better than LTP  $L_2$ -Grassmann. Both  $L_1$  and  $L_2$  LTP Grassmann reached 100% recognition accuracy on the Yale Figure 46, extended Yale B Figure 48 and the AR databases Figure 49. LTP  $L_1$ -Grassmann outperformed LTP  $L_2$ -Grassmann by 0.63% on the AT&T database Figure 47, 3.23% on the LFW database Figure 50, 2.25% on the Cohn-Kanade database Figure 51 and 1.75% on the extended Cohn-Kanade database Figure 52.

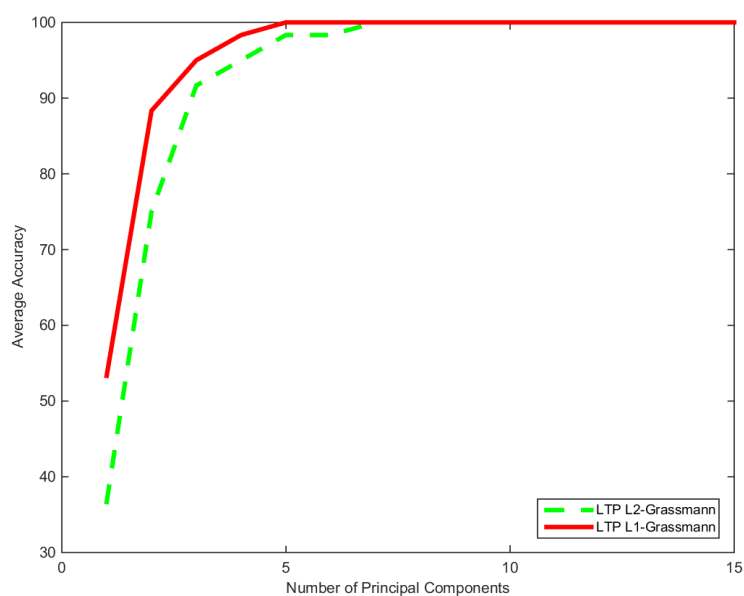


Figure 46: LTP Grassmann Yale Database ( $t = 5$ )

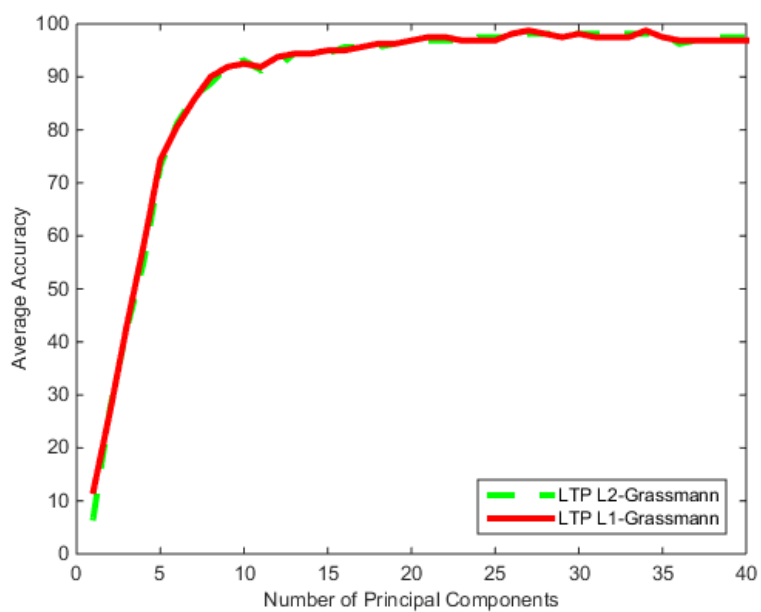
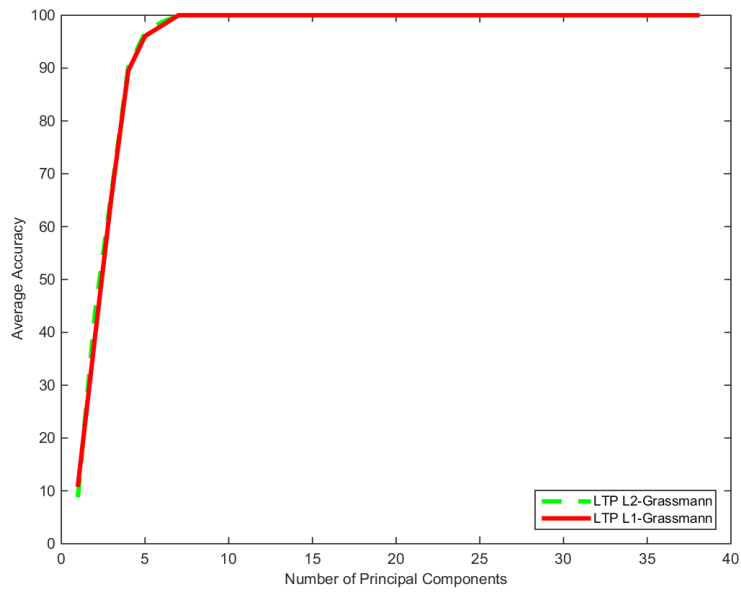
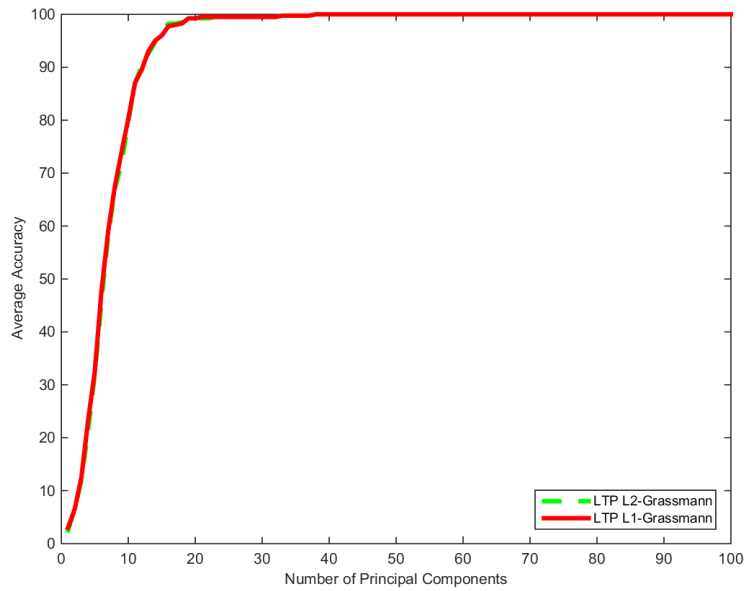


Figure 47: LTP Grassmann AT&T Database ( $t = 6$ )



**Figure 48: LTP Grassmann Extended Yale B Database ( $t = 5$ )**



**Figure 49: LTP Grassmann AR Database ( $t = 5$ )**

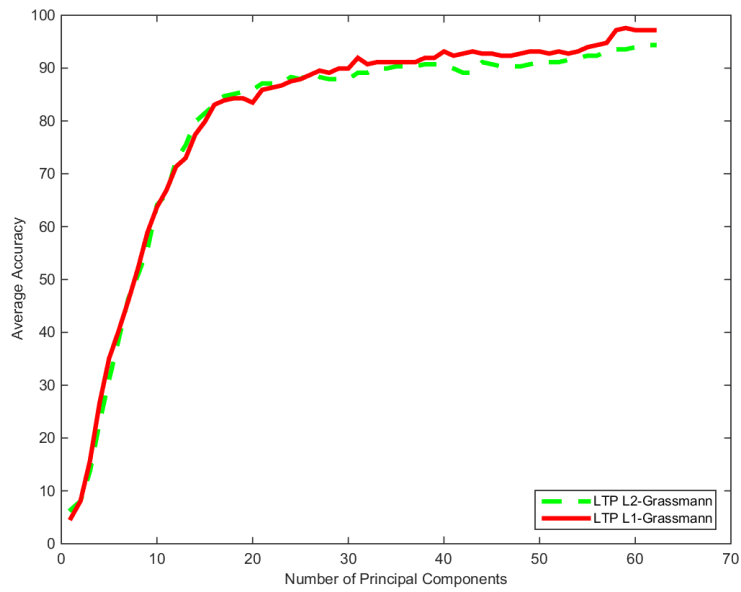


**Figure 50: LTP Grassmann LFW Database ( $t = 5$ )**

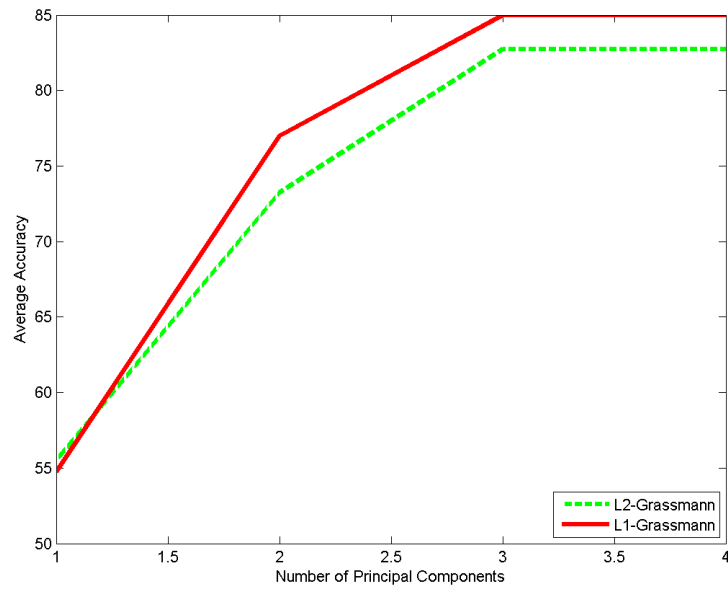


**Figure 51: LTP Grassmann Cohn-Kanade Database ( $t = 14$ )**

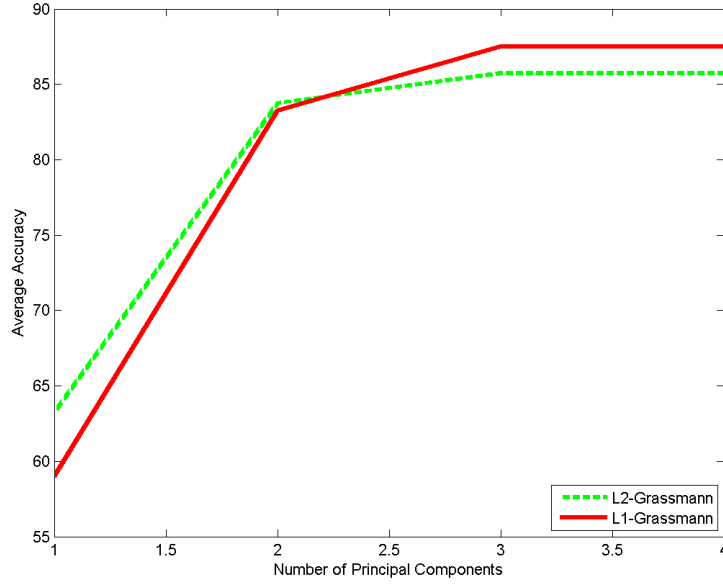


**Figure 52: LTP Grassmann Extended Cohn-Kanade Database ( $t = 16$ )**

This indicates that databases with a small amount of noise or a large number of data samples may get the similar results as LTP  $L_1$ -Grassmann. Conversely, datasets with large amounts of noise like LFW or a small number of data samples like the Cohn-Kanade database get better results with LTP  $L_1$ -Grassmann. Another interesting observation from these results is that the optimal LTP value is much larger for expression recognition. The larger LTP most likely removes some of the finer features of the faces that are not need for expression recognition but are need for face recognition.

In the final experiment LTP  $L_1$ -Grassmann was run on a varying number of images per subjects from LFW database. This experiment is repeated ten times and the average accuracy is reported. This test is meant to evaluate the effect of the number of data samples on accuracy.



The results in Figure 53 show that LTP  $L_2$ -Grassmann can handle the traditional noise of LFW given enough data samples. However, as more data samples are removed from the subspaces  $L_2$ -PCA becomes more sensitive to the inherent noise and as a result  $L_1$ -Grassmann gains a clear advantage.

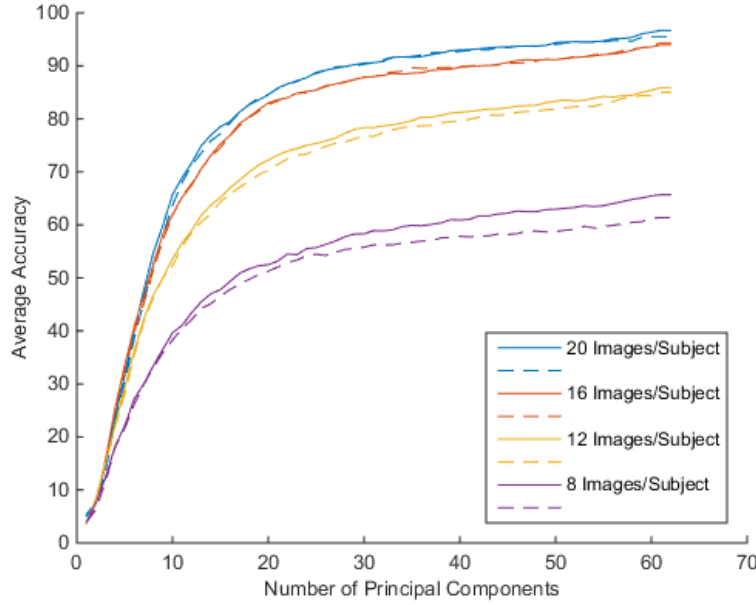


**Figure 53: LTP Grassmann Comparison on Varying number of Subject Images**  
**Solid: LTP  $L_1$ -Grassmann and Dashed: LTP  $L_2$ -Grassmann**

#### 4.5. Accuracy State of the Art

In this section we compare the classification accuracies of LTP  $L_1$ -Eigenfaces and LTP  $L_1$ -Grassmann against state of the art methods on the Yale, AT&T, extended Yale B, and AR datasets. LFW is excluded from this section because testing involves determining if a pair of face images are a match. This test methodology is significantly different from the methodology used throughout this thesis.

The LTP  $L_1$ -Grassmann results are difficult to compare to existing techniques because many methods compare individual test samples against a trained set rather than groups of unknown test samples of the same class. Methods that utilize individual test samples will be marked with “Single” and methods that utilize groups of unknown test samples will be marked with “Many”. Top performing methods will be indicated with bold accuracy, excluding “Many” results which are expected to classify better than the “Single” methods.

#### 4.5.1 Yale Face Database

For the Yale Face database the 4 fold cross validation results are reported in Table 2. LTP  $L_1$ -Eigenfaces was outperformed by the state of the art by 4.81%. The current state of the art was developed by Stentiford in [37] and recognizes individuals by matching cliques of points between face graphs. The next closest competitive method was by Cevikalp et al. [38] which introduces discriminative common vectors, a variant of LDA that can be directly applied to datasets with small sample sizes.

Method	Testing Method	Classification Accuracy
LTP $L_1$ -Eigenface	single	95.19%
LTP $L_1$ -Grassmann	many	100.00%
Cevikalp et al. [38]	single	97.33%
Yang [39]	single	93.94%
Stentiford [37]	single	<b>100.00%</b>
Zhou et al. [40]	single	96.67%
Abdullah et al. [41]	single	97.25%

Table 2: State of the Art Comparison for Yale Face Database

### 4.5.2 AT&T Database of Faces

For the AT&T Database of Faces the 4 fold cross validation results are reported in Table 3. LTP  $L_1$ -Eigenfaces was outperformed by the state of the art by 10.97% and LTP  $L_1$ -Grassmann was outperformed by 3.75%. The leading method is presented by Othman et al. in [42] in which they use 2D-Hidden Markov Models perform recognition using the image pixels as features. The next closest competitive method was by Lenc in [43] in which they identify key-points from Gabor wavelet using k-means with LBP.

Method	Testing Method	Classification Accuracy
LTP $L_1$ -Eigenface	single	88.83%
LTP $L_1$ -Grassmann	many	96.25%
Azary [44]	single	99.00%
Azary [44]	many	100.00%
Faraji & Qi [45]	single	98.87%
Othman et al. [42]	single	<b>100%</b>
Lenc & Král [43]	single	99.80%

Table 3: State of the Art Comparison for AT&T Database of Faces

### 4.5.3 Extended Yale Face Database B

The leading method is presented by Kumar et al. in [46] in which they learn a series of convolution filters to extract features and then apply boosting to perform recognition. The next closest competitive method was by Azary in [44] in which he utilizes Grassmannian Sparse Representations for “Single” and Grassmannian Spectral Regression for “Many” tests.

Method	Testing Method	Classification Accuracy
LTP $L_1$ -Grassmann	many	100.00%
Azary [44]	single	98.89%
Azary [44]	many	100.00%
Fernandes & Bala [47]	single	97.50%
Cai et al. [48]	single	95.17%
Kumar et al. [46]	single	<b>99.6%</b>

Table 4: State of the Art Comparison for Extended Yale B Face Database

#### 4.5.4 AR Face Database

For the AR Database of Faces the 4 fold cross validation results are reported in Table 5. LTP  $L_1$ -Grassmann outperformed state of the art by 21.69%, however state of the art utilized the “Single” testing methodology. The leading method is presented by Andrés et al. in [49] in which they detect the occlusions and utilize the non-occluded regions to perform recognition. The next closest competitive method was by Liu et al. [50] which reports 95.30% accuracy on the AR Database of Faces using  $L_2$ -norm regularization to learn a dictionary more suitable for face recognition from face reconstruction error.

Method	Testing Method	Classification Accuracy
LTP $L_1$ -Grassmann	many	100.00%
Xuefeng et al. [51]	single	95.20%
Lin et al. [52]	single	91.50%
Martinez [53]	single	85.00%
Andrés et al. [49]	single	<b>98.31%</b>
Liu et al. [50]	single	95.30%

Table 5: State of the Art Comparison for AR Face Database

## 4.6. Speed tests

For the GPU benchmark the number of data samples was varied to see how each implementation scaled to larger datasets. All the images were taken from the labeled faces in the wild dataset and were cropped such that only the face was visible [54]. Images were added incrementally to form test sets with varying number of samples and each test set is scaled and centered before running  $L_1$ -PCA. The timing is collected for the first fifty eigenvectors of each test set. For test sets with fewer eigenvectors the timing is repeated ten times to get the average performance time. All performance experiments were performed on a 64-bit Windows 7 machine with an Intel Core i5-2400 3.10-GHz CPU and 8 GB of RAM. The NVIDIA GTX 480 and NVIDIA Tesla K20c were used for GPU experiments, both used the CUDA 5.0 driver.

As expected the time complexity of the  $L_1$ -PCA algorithm is quadratic in relation to the number of data samples as shown in Figures 54, 55 and 56. The CPU runtime is several orders of magnitude larger than the GTX and Tesla runtime.

The GTX speedup varies from 2x to 9.4x and the Tesla speedup is from 7.4x to 21.5x faster as shown in Figures 57 and 58. In both speedup graphs there are data points where the performance suddenly drops. These performance drops indicate that the GPU utilization has decreased and are the result of edge cases between block sizes. The drop in performance occurs at 960 data samples on the GTX where the block size is 768. With that block size there will be 1 block with full utilization and a second block with 75% of the threads being stalls. Similarly a drop in performance occurs at 1280 data samples on the Tesla card where the block size is 1024.

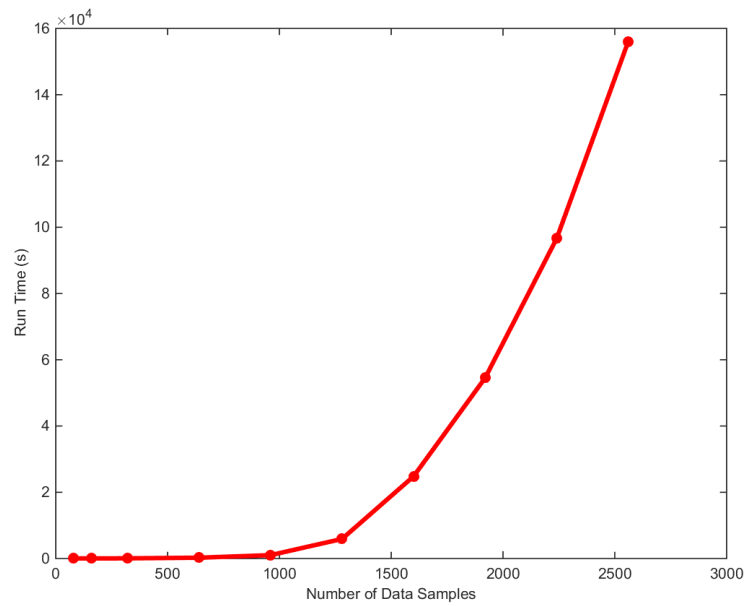


**Figure 54: CPU Timing**

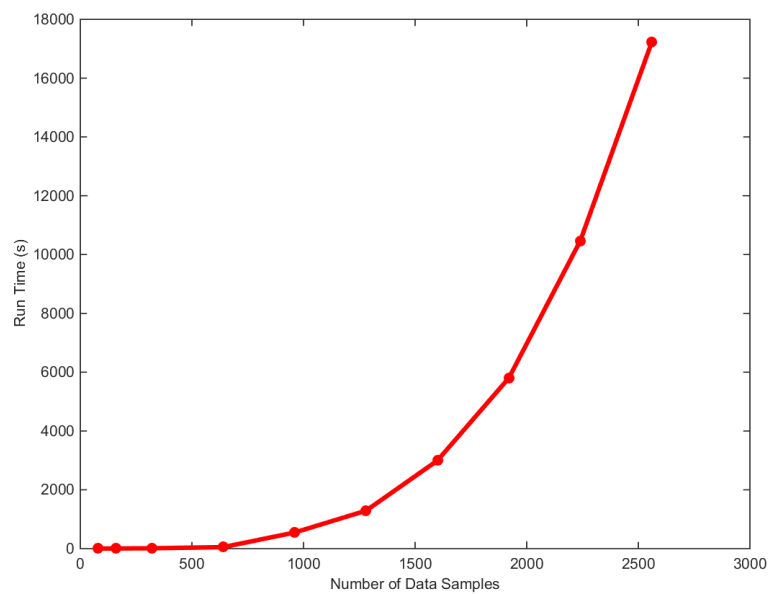


**Figure 55: GTX Timing**

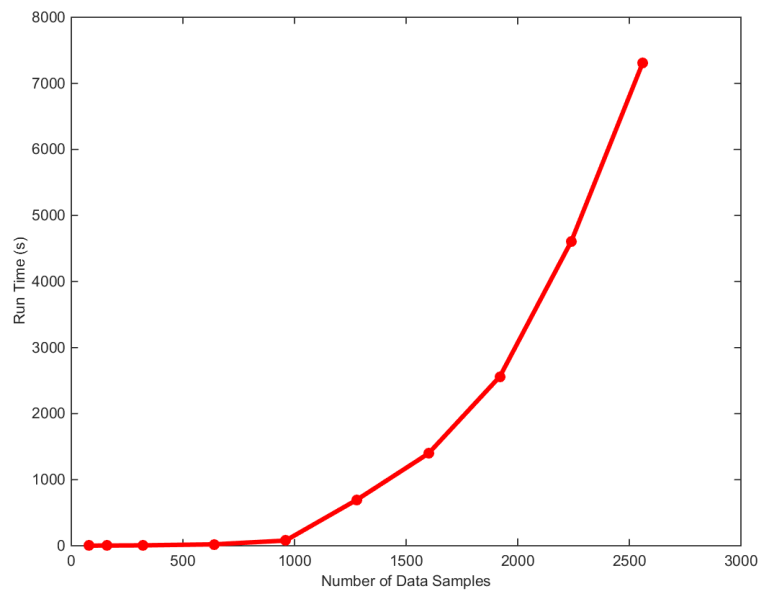


**Figure 56: Tesla Timing**

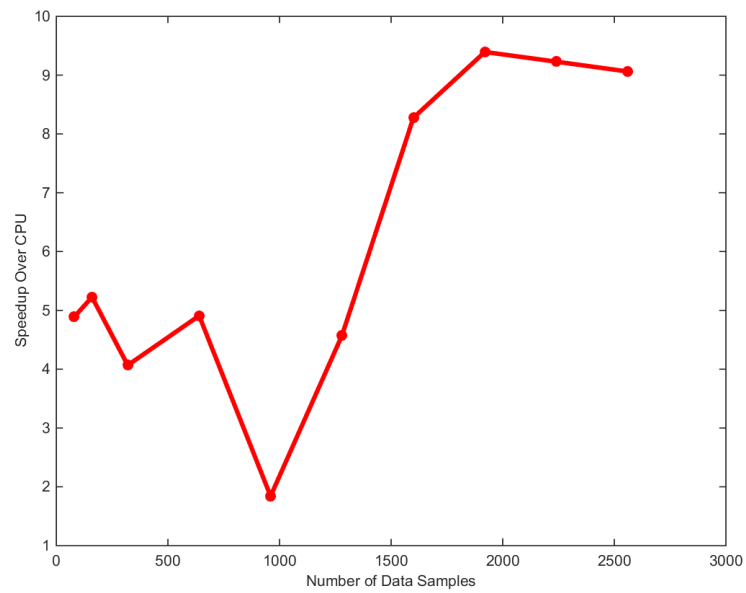


**Figure 57: GTX Speedup**

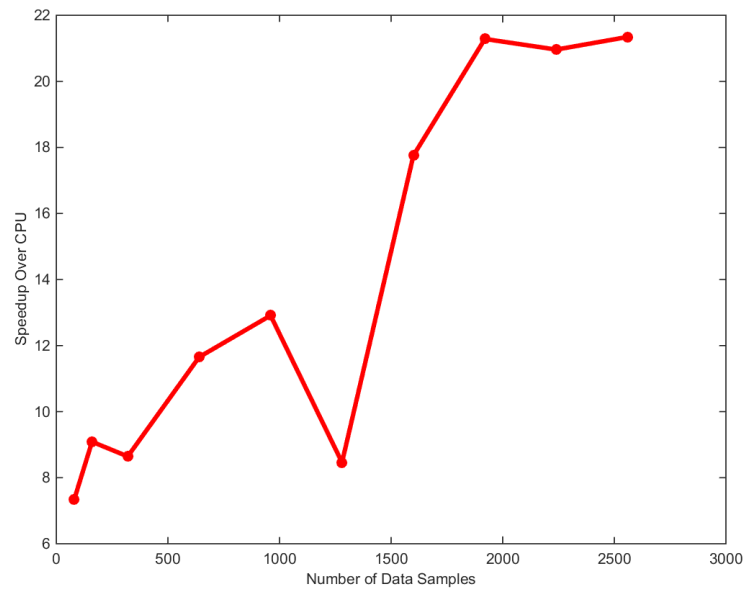


**Figure 58: Tesla Speedup**



## Chapter 5 Conclusion and Future Work

The aim of this thesis was to develop recognition algorithms that leverages  $L_1$ -PCA to improve accuracy in unconstrained environments. The following contributions to the field of recognition were presented in this work:

- An extension of an  $L_1$  Principal Component algorithm to multiple components
- A high performance implementation of  $L_1$ -PCA on GPU using CUDA
- An  $L_1$ -PCA mapping for Grassmann manifolds
- An extension of  $L_1$ -Grassmann using LTP

Despite the suboptimal methods that were employed for  $L_1$ -PCA, recognition accuracy was not negatively affected for clean images. Furthermore,  $L_1$ -eigenfaces outperformed  $L_2$ -eigenfaces when occlusions were added to the data, which indicates that  $L_1$ -PCA is more robust to outliers. The results also show that the proposed  $L_1$ -Grassmann approach outperformed the traditional  $L_2$ -Grassmann method for face recognition of clean and occluded faces. This indicates that mapping to the Grassmann manifold is very sensitive to noise and benefits from the more robust mapping systems. Additionally,  $L_1$ -Grassmann has been generic enough to be applied to other recognition tasks such as facial expression recognition. This work has also shown that the proposed  $L_1$ -PCA algorithm can greatly benefit from a GPU implementation. The high performance implementation was several times faster than the CPU based  $L_1$ -PCA techniques allowing it to run on larger datasets in a reasonable amount of time. Lastly the LTP preprocessing removed the effects of varying illumination and improved the accuracy of both techniques on databases with large variations in illumination.

One problem that plagues the suboptimal  $L_1$ -PCA, is that the later eigenvectors tend to capture the noise in the images. This is caused by the suboptimal greedy search removing good features until there is nothing, but noise left. This factor leads to complications when many eigenvectors are needed for applications such as  $L_1$ -Eigenfaces. If too many eigenvectors are used, the noise in the image will begin to affect the results and performance will become similar to  $L_2$ -eigenfaces. Conversely, if too few eigenvectors are used, the features will not be specific enough to distinguish between subjects. Thus, the best performance is achieved with a modest number of eigenvectors. The potential solution is to develop an algorithm that solves for all  $L_1$ -eigenvectors simultaneously. However, this fundamentally changes the contribution calculation such that the bit-flip algorithm would no longer work. In the past, authors have used an exhaustive search over  $2^{NM}$  binary matrices of size  $N \times M$ , where  $N$  is the number of data samples and  $M$  is the number of eigenvectors to solve for all  $L_1$ -eigenvectors simultaneously [9].

Additionally the Grassmann algorithm has experienced difficulty recognizing subjects when there are few training or test images per subject. Several images of the subject are needed to properly map images to points on the Grassmann. Too few images causes the points on the Grassmann to be too general which results in poor performance. One potential method for mitigating such a problem is to artificially expand the number of images using techniques like affine transformation. This would allow the Grassmann manifold to capture the in-class variability for sparse classes and improve performance.

In conclusion, this work has demonstrated that  $L_1$ -PCA improves the robustness of recognition techniques such as Eigenfaces and Grassmann learning. Furthermore

experimental results have shown that  $L_1$ -PCA has the potential to be greatly accelerated using the GPGPU.

## Bibliography

- [1] R. Jafri and H. R. Arabnia, "A Survey of Face Recognition Techniques," *JIPS*, vol. 5, no. 2, pp. 41-68, 2009.
- [2] N. Funatsu and Y. Kuroki, "Fast parallel processing using GPU in computing L1-PCA bases," *TENCON*, pp. 2087-2090, 2010.
- [3] J. Hamm and D. D. Lee, "Grassmann discriminant analysis: a unifying view on subspace-based learning," *Proceedings of the 25th international conference on Machine learning*, pp. 376-383, 2008.
- [4] P. Turaga, A. Veeraraghavan and R. Chellappa, "Statistical analysis on Stiefel and Grassmann manifolds with applications in computer vision," *Computer Vision and Pattern Recognition*, pp. 1-8, 2008.
- [5] K. Pearson, "On Lines and Planes of Closest Fit to Systems," *The London, Edinburgh, and Dublin Philosophical Magazine and Journal of Science*, vol. 2, no. 11, pp. 559-572, 1901.
- [6] J. Shlens, "A Tutorial on Principal Component Analysis," *CoRR*, vol. abs/1404.1100, 2014.
- [7] P. P. Markopoulos, G. Karystinos and D. Pados, "Some options for L1-subspace signal processing," *Proc. Tenth Int. Symposium on Wireless Communication Systems*, 2013.
- [8] N. Kwak, "Principal Component Analysis Based on L1-norm Maximization," *IEEE Transactions on Pattern Analysis and Machine Intelligence, PAMI*, 2008.

- [9] P. P. Markopoulos, G. N. Karystinos and D. A. Pados, "Optimal Algorithms for L1-subspace Signal Processing," *IEEE Transactions on Signal Processing*, 2013.
- [10] Q. Ke and T. Kanade, "Robust L1 Factorization in the Presence of Outliers and Missing Data by Alternative Convex Programming," *CVPR*, pp. 739-746, 2005.
- [11] F. Nie, H. Huang, C. Ding, D. Luo and H. Wang, "Robust principal component analysis with non-greedy l1-norm maximization," *IJCAI Proc. Int. Joint Conference on Artificial Intelligence*, vol. 22, no. 1, 2011.
- [12] S. Kundu, P. P. Markopoulos and D. A. Pados, "Fast computation of the L1-principal component of real-valued data," *Proceedings of 39th IEEE International Conference on Acoustics Speech and Signal Processing, ICASSP*, 2014.
- [13] M. Kirby and L. Sirovich, "Application of the Karhunen-Loeve Procedure for the Characterization of Human Faces," *IEEE Transactions on Pattern Analysis and Machine Intelligence*, vol. 12, no. 1, pp. 103-108, 1990.
- [14] M. Turk and A. Pentland, "Face recognition using eigenfaces," *IEEE Conference on Computer Vision and Pattern Recognition, CVPR*, 1991.
- [15] A. Pentland, B. Moghaddam and T. Starner, "View-based and modular eigenspaces for face recognition," *Computer Vision and Pattern Recognition*, vol. CVPR'94, 1994.
- [16] R. Gottumukkal and V. K. Asari, "An improved face recognition technique based on modular PCA approach," *Pattern Recognition Letters*, vol. 25, no. 4, pp. 429-436, 2004.
- [17] J. Yang, D. Zhang, A. Frangi and J.-y. Yang, "Two-dimensional PCA: a new

- approach to appearance-based face representation and recognition," *Pattern Analysis and Machine Intelligence*, vol. 26, no. 1, pp. 131-137, 2004.
- [18] R. Shigenaka, B. Raytchev, T. Tamaki and K. Kaneda, "Face sequence recognition using Grassmann distances and Grassmann kernels," *Neural Networks (IJCNN)*, pp. 1-7, 2012.
- [19] S. Azary and A. Savakis, "Grassmannian Sparse Representations and Motion Depth Surfaces for 3D Action Recognition," *Computer Vision and Pattern Recognition Workshops (CVPRW)*, 2013.
- [20] T. Ojala, M. Pietikainen and T. Maenpaa, "Multiresolution Gray Scale and Rotation Invariant Texture Classification," *Pattern Analysis Machine Intelligence*, vol. 24, no. 7, pp. 971-987, 2002.
- [21] X. Tan and B. Triggs, "Enhanced Local texture Feature Sets for Face Recognition Under Difficult Lighting Conditions," *Transactions on Image Processing*, vol. 19, no. 6, pp. 1635-1650, 2010.
- [22] NVIDIA, "CUDA C Programing Guide v6.0," 13 February 2014. [Online]. Available: <http://docs.nvidia.com/cuda/cuda-c-programming-guide/index.html#axzz36kgvGYg4>.
- [23] F. Zhong, "L1-norm-based (2D)<sup>2</sup>PCA," *Conference on Computer Science and Electrical Engineering*, pp. 1293-1296, 2013.
- [24] T. Shkunaga and K. Shigenari, "Decomposed eigenface for face recognition under various lighting conditions," *Proceedings of the 2001 IEEE Conference on Computer Vision and Pattern Recognition, CVPR*, 2001.

- [25] P. Belhumeur, J. Hespanha and D. Kriegman, "Eigenfaces vs. fisherfaces: Recognition using class specific linear projection," *IEEE Transactions on Pattern Analysis and Machine Intelligence, PAMI*, pp. 711-720, 1997.
- [26] D. Roy, "The Normalized Yale Face Database," MIT, 01 September 2000. [Online]. Available: <http://vismod.media.mit.edu/vismod/classes/mas622-00/datasets/>.
- [27] F. S. Samaria and A. C. Harter, "Parameterisation of a stochastic model for human face identification," *Applications of Computer Vision*, pp. 138-142, 1994.
- [28] A. S. Georgiades, P. N. Belhumeur and D. J. Kriegman, "From Few to Many: Illumination Cone Models for Face Recognition under Variable Lighting and Pose," *IEEE Transactions on Pattern Analysis and Machine Intelligence*, vol. 23, pp. 643-660, 2001.
- [29] A. M. Martinez and R. Benavente, "The AR Face Database," 1998.
- [30] G. B. Huang, M. Ramesh, T. Berg and E. Learned-Miller, "Labeled Faces in the Wild: A Database for Studying," University of Massachusetts, Amherst, 2007.
- [31] P. Viola and M. J. Jones, "Robust real-time face detection," *International journal of computer vision*, vol. 57, no. 2, pp. 137-154, 2004.
- [32] G. Huang, M. Mattar, H. Lee and E. G. Learned-Miller, "Learning to align from scratch," *Advances in Neural Information Processing Systems*, pp. 764-772, 2012.
- [33] T. Kanade, J. F. Cohn and Y. Tian, "Comprehensive database for facial expression analysis," *Proceedings of the Fourth IEEE International Conference on Automatic Face and Gesture Recognition*, pp. 46-53, 2000.
- [34] P. Lucey, J. F. Cohn, T. Kanade, J. Saragih, Z. Ambadar and I. Matthews, "The

- Extended Cohn-Kanade Dataset (CK+): A complete expression dataset for action unit and emotion-specified expression," *Proceedings of the Third International Workshop on CVPR for Human Communicative Behavior Analysis* , pp. 94-101, 2010.
- [35] Z. Wang, R. Huang, W. Yang and C. Sun, "An enhanced Local Ternary Patterns method for face recognition," *Control Conference*, vol. 33, pp. 4636-4640, 2014.
- [36] S. Jung and J. S. Marron, "PCA consistency in high dimension, low sample size context," *The Annals of Statistics*, vol. 37, no. 6B, pp. 4104-4130, 2009.
- [37] F. Stentiford, "Face recognition by detection of matching cliques of points," *IS&T/SPIE Electronic Imaging*, 2014.
- [38] H. Cevikalp, M. Neamtu, M. Wilkes and A. Barkana, "Discriminative common vectors for face recognition," *Pattern Analysis and Machine Intelligence*, vol. 27, no. 1, pp. 4-13, 2005.
- [39] M.-H. Yang, "Kernel eigenfaces vs. kernel fisherfaces: Face recognition using kernel methods," *Automatic Face and Gesture Recognition*, vol. 10, pp. 0215-0215, 2013.
- [40] L. Zhou, Y. Xu, Z.-M. Lu and T. Nie, "Face recognition based on multi-wavelet and sparse representation," *J. Inf. Hiding Multimed. Signal Process*, vol. 5, no. 3, pp. 399-407, 2014.
- [41] M. F. A. Abdullah, M. S. Sayeed, K. S. Muthu, H. K. Bashier, A. Azman and S. Z. Ibrahim, "Face recognition with symmetric local graph structure (slgs)," *Expert Systems with Applications*, vol. 41, no. 14, pp. 6131-6137, 2014.
- [42] H. Othman and T. Aboulnasr, "A separable low complexity 2D HMM with



- application to face recognition," *Pattern Analysis and Machine Intelligence*, vol. 25, no. 10, pp. 1229-1238, 2003.
- [43] L. Lenc and P. Král, "Automatically Detected Feature Positions for LBP Based Face Recognition," *Artificial Intelligence Applications and Innovations*, pp. 246-255, 2014.
- [44] S. Azary, "Grassmann Learning for Recognition and Classification," Rochester Institute of Technology, Rochester, 2014.
- [45] M. R. Faraji and X. Qi, "An effective neutrosophic set-based preprocessing method for face recognition," *Multimedia and Expo Workshops*, 2013.
- [46] R. Kumar, A. Banerjee, B. Vemuri and H. Pfister, "Trainable convolution filters and their application to face recognition," *Pattern Analysis and Machine Intelligence*, vol. 7, no. 34, pp. 1423-1436, 2012.
- [47] S. Fernandes and J. Bala, "Performance Analysis of PCA-based and LDA-based Algorithms for Face Recognition," *Signal Processing Systems*, vol. 1, no. 1, pp. 1-6, 2013.
- [48] D. Cai, X. He, J. Han and H. Zhang, "Orthogonal laplacianfaces for face recognition," *Image Processing*, vol. 15, no. 11, pp. 3608-3614, 2006.
- [49] M. A. Andrés, S. Padovani, M. Tepper and J. Jacobo-Berlles, "Face recognition on partially occluded images using compressed sensing," *Pattern Recognition Letters*, vol. 36, pp. 235-242, 2014.
- [50] H.-D. Liu, M. Yang, Y. Gao, Y. Yin and L. Chen, "Bilinear discriminative dictionary learning for face recognition," *Pattern Recognition*, vol. 47, no. 5, pp. 1835-1845,

2014.

- [51] C. Xuefeng, L. Fei and C. Huang, "Face recognition by Zero-Ratio based LGBP features," *Intelligent Control and Automation (WCICA)*, vol. 11, pp. 5605-5608, 2014.
- [52] J. Lin, J. Ming and D. Crookes, "Robust face recognition with partially occluded images based on a single or a small number of training samples," *Speech and Signal Processing*, pp. 881-884, 2009.
- [53] A. M. Martínez, "Recognizing imprecisely localized, partially occluded, and expression variant faces from a single sample per class," *Pattern Analysis and Machine Intelligence*, vol. 24, no. 6, pp. 748-763, 2002.
- [54] B. Gary, H. Ramesh, M. Ramesh, T. Berg and E. Learned-Miller, "Labeled Faces in the Wild: A Database for Studying," University of Massachusetts, Amherst, 2007.
- [55] M. Johnson and A. Savakis, "Fast L1-eigenfaces for robust face recognition," *Western New York Image and Signal Processing Workshop (WNYISPW)*, 2014.